

# TOPOLOGICAL PHASES ON LIEB LATTICE

A Thesis

submitted to

Indian Institute of Science Education and Research Pune

in partial fulfillment of the requirements for the

BS-MS Dual Degree Programme

by

Anirban Sharma

**20121049**



Indian Institute of Science Education and Research Pune

Dr. Homi Bhabha Road,  
Pashan, Pune 411008, INDIA.

April, 2017

Supervisor: Dr. Mukul Laad


© Anirban Sharma 2017

All rights reserved

# Certificate

This is to certify that this thesis entitled "Topological Phases on Lieb Lattice" submitted towards the partial fulfilment of the BS-MS dual degree programme at the Indian Institute of Science Education and Research Pune represents original research carried out by Anirban Sharma at Institute of Mathematical Science, under the supervision of Dr. Mukul Laad during the academic year 2016-2017.

Student  
ANIRBAN  
SHARMA

  
30/3/2017  
Supervisor  
DR. MUKUL S  
LAAD

# Declaration

I hereby declare that the matter embodied in the report entitled 'Topological phases on Lieb lattice' are the results of the investigations carried out by me at the Department of Physics, Institute of Mathematical Sciences, Chennai under the supervision of Dr. Mukul S Laad and the same has not been submitted elsewhere for any other degree.

*A Sharma*  
30/3/2017

Student  
ANIRBAN  
SHARMA

*M S Laad*  
30/3/2017

Supervisor  
MUKUL S LAAD

# Acknowledgements

I am extremely grateful to Dr. Mukul S Laad for providing me an opportunity to work with him at Institute of Mathematical Sciences, Chennai. I would like to thank him for the amount of time spent in explaining me the intricacies of the problem and lessons on how to go about a problem. It was a great learning experience.

I would like to thank Dr. Mukul Kabir for his interest. I highly appreciate the amount of time he spent to discuss problems with me. It was great having conversations with him.

I would like to thank Dr. Rejish Nath for his constant support throughout my IISER life.

I would like to express my gratitude towards the Physics Department, IISER for providing me an opportunity to carry out the project at IMSc.

Finally, I would like to thank my parents, brother and friends for their constant mental and emotional support. I would like to dedicate the thesis to my parents.

# Abstract

We show that a Mott transition is possible in our model with a dimer placed on each site of a Lieb lattice. To illustrate this, we map the lattice problem to an impurity problem. Then we solve the impurity problem to show the Mott transition. We then investigate the band structure of the non-interacting problem using the tight binding approximation. We show that the band structure is topologically non-trivial. To check the stability of BCPs, we introduce different hoppings. We get quadratic band crossing points(QBCPs), tilted Dirac cones in the band structure. Then we introduce the electric field in the system in z direction to see the effect of inversion symmetry breaking. As the inversion symmetry is broken, we then introduce Rashba spin orbit coupling type interaction in the Hamiltonian to check its effect on the BCPs. Finally, the model is mapped to a two orbital per site model. We are able to show that the topologically non-trivial features can be found in a system having an odd and an even parity orbital at each site.

# Contents

<b>1</b>	<b>Introduction</b>	<b>9</b>
<b>2</b>	<b>Theory</b>	<b>11</b>
2.1	Many Body Physics . . . . .	11
2.1.1	Green's function . . . . .	11
2.1.2	Feynman Diagrams . . . . .	14
2.1.3	Dyson's Equation . . . . .	15
2.2	Band Topology . . . . .	16
2.2.1	Berry Phase . . . . .	16
<b>3</b>	<b>Methods</b>	<b>20</b>
3.1	Dynamical Mean Field Theory . . . . .	20
3.1.1	Motivations for using infinite dimensions . . . . .	20
3.1.2	Classical Spin Model . . . . .	21
3.1.3	Hubbard model in high dimensions . . . . .	21
3.2	Equation of Motion for Green's function . . . . .	23
3.3	Falicov-Kimball Model . . . . .	23
3.4	Metal-insulator transition . . . . .	24
<b>4</b>		<b>26</b>
4.1	Model . . . . .	26
4.2	Effects of Additional Hopping . . . . .	31
4.2.1	Results . . . . .	32
4.2.2	Diagonal hopping . . . . .	43
4.3	Effects of Electric Field . . . . .	44
4.3.1	Results . . . . .	45
4.4	Rashba term . . . . .	46
4.5	Haldane Model . . . . .	49
<b>5</b>	<b>Extensions of the model</b>	<b>51</b>
5.1	Two-orbital model . . . . .	51

<b>6 Discussion</b>	<b>65</b>
6.1 Mean-field Theory . . . . .	66

# List of Figures

4.1	Lieb lattice and the model with intra dimer and one inter dimer hopping . . . . .	26
4.2	a)Mott-transition in the DOS b)Self energy for parameters $t = t'$ [1] . . . . .	28
4.3	Dispersion relation for staggered case for a) $a_+$ bands b) $a_-$ bands with parameters ( $t = 1, t' = 1.0, t'' = 0.5, V_1 = V_3 = 0, V_2 = 1$ ) . . . . .	32
4.4	Cross section of the band structure through the a)plane $k_x = \pi$ and b)the diagonal plane ( $k_x = k_y$ ) with parameters $t = 1, t' = 1.0, t'' = 0.5, V_1 = V_3 = 0, V_2 = 1$ . The band crossing point of the two lower $a_+$ bands at $(\pi, \pi)$ is a QBCP. Two $a_-$ bands touch at a surface. . . . .	33
4.5	Fermi surface for the $a_+$ bands for Von-Hove singularity at a) $\omega = -4.275$ and at b) $\omega = -1.3659$ for parameters $t = 1, t' = 1.0, t'' = 0.5, V_1 = V_3 = 0, V_2 = 1$ . . . . .	33
4.6	Fermi surface for the $a_+$ bands for Von-Hove singularity at a) $\omega = 0.488$ and for the $a_-$ bands at b) $\omega = 0.5$ for parameters $t = 1, t' = 1.0, t'' = 0.5, V_1 = V_3 = 0, V_2 = 1$ . . . . .	34
4.7	Fermi surface for $a_-$ bands with ( $t = 1, t' = 1.0, t'' = 0.5, V_1 = V_3 = 0, V_2 = 1$ ) for Von-Hove singularity at a) $\omega = 1.4809$ and b) $\omega = 2$ . . . . .	34
4.8	a)Fermi surface for $a_-$ with ( $t = 1, t' = 1.0, t'' = 0.5, V_1 = V_3 = 0, V_2 = 1$ ) for Von-Hove singularity at $\omega = 1.4809$ and b)DOS for all the bands. . . . .	35
4.9	Dispersion relation for symmetric case for (a) $a_+$ bands and (b) $a_-$ bands with parameters $V_1 = V_2 = V_3 = 1, t = 1, t' = 0.75, t'' = -0.5$ . . . . .	35
4.10	Cross section of the band structure for through a)plane $k_x = \pi$ and b) plane $k_x = k_y$ with parameters $V_1 = V_2 = V_3 = 1, t = 1, t' = 0.75, t'' = -0.5$ . . . . .	36



4.11	DOS for a) $a_+$ and b) $a_-$ bands with parameters $V_1 = V_2 = V_3 = 1, t = 1, t' = 0.75, t'' = -0.5$ . . . . .	36
4.12	Fermi surface for symmetric case for lower bands with $(t = 1, t' = 0.75, t'' = -0.5)$ for Von-Hove singularity at $\omega = -3.266$ . . . . .	37
4.13	Fermi surface for symmetric case for lower bands with $(t = 1, t' = 0.75, t'' = -0.5)$ for Von-Hove singularity at $\omega = 0.276$ . . . . .	37
4.14	Fermi surface for symmetric case for lower bands with $(t = 1, t' = 0.75, t'' = -0.5)$ for Von-Hove singularity at $\omega = 1.486$ . . . . .	37
4.15	Fermi surface for symmetric case for lower bands with $(t = 1, t' = 0.75, t'' = -0.5)$ for Von-Hove singularity at $\omega = 1.926$ . . . . .	37
4.16	Fermi surface for symmetric case for top bands with $(t = 1, t' = 0.75, t'' = -0.5)$ for Von-Hove singularity at $\omega = 1.992$ . . . . .	38
4.17	Fermi surface for symmetric case for top bands with $(t = 1, t' = 0.75, t'' = -0.5)$ for Von-Hove singularity at $\omega = 2.244$ . . . . .	38
4.18	Fermi surface for symmetric case for top bands with $(t = 1, t' = 0.75, t'' = -0.5)$ for Von-Hove singularity at $\omega = 2.496$ . . . . .	38
4.19	Fermi surface for symmetric case for top bands with $a(t = 1, t' = 0.75, t'' = -0.5)$ for Von-Hove singularity at $\omega = 2.76$ . . . . .	38
4.20	DOS(zoomed view) for symmetric case with $t = 1, t' = 0.75, t'' = -0.5$ . . . . .	38
4.21	Band structure for a) $a_+$ and b) $a_-$ bands with parameters $V_1 = V_2 = V_3 = 1, t = 1, t' = 1, t'' = -0.5$ . . . . .	39
4.22	Cross section of the band dispersions for through the plane $k_x = \pi$ with $(t = 1, t' = 1.0, t'' = -0.5)$ . . . . .	39
4.23	Cross section of the band dispersions for through the diagonal plane $k_x = k_y$ with $(t = 1, t' = 1.0, t'' = -0.5)$ . . . . .	40
4.24	DOS for symmetric case for $a_-$ bands $(t = 1, t' = 1.0, t'' = -0.5)$ . . . . .	40
4.25	DOS for symmetric case for $a_+$ bands $(t = 1, t' = 1.0, t'' = -0.5)$ . . . . .	40
4.26	Fermi surface for symmetric case for $a_+$ bands $(t = 1, t' = 1.0, t'' = -0.5)$ for Von-Hove singularity at $\omega = -4.27$ . . . . .	41
4.27	Fermi surface for symmetric case for $a_-$ bands with $(t = 1, t' = 1.0, t'' = -0.5)$ for Von-Hove singularity at $\omega = 0.27$ . . . . .	41
4.28	Fermi surface for symmetric case for $a_+$ bands $(t = 1, t' = 1.0, t'' = -0.5)$ for Von-Hove singularity at $\omega = 1.5$ . . . . .	41
4.29	Fermi surface for symmetric case for $a_+$ bands $(t = 1, t' = 1.0, t'' = -0.5)$ for Von-Hove singularity at $\omega = 2$ . . . . .	41
4.30	Fermi surface for symmetric case for $a_-$ band with $t = 1, t' = 1.0, t'' = -0.5$ for Von-Hove singularity at $\omega = 2.1$ . . . . .	42
4.31	Fermi surface for symmetric case for $a_-$ band with $t = 1, t' = 1.0, t'' = -0.5$ for Von-Hove singularity at $\omega = 2.35$ . . . . .	42

4.32	Fermi surface for symmetric case for $a_-$ bands with $t=1, t'=1.0, t''=-0.5$ for Von-Hove singularity at $\omega = 2.4865$ . . . . .	42
4.33	Fermi surface for symmetric case for $a_-$ bands with ( $t = 1, t' = 1.0, t'' = -0.5$ ) for Von-Hove singularity at $\omega = 3.75$ . . . . .	43
4.34	Cross section of the band dispersions for through the diagonal plane a) $k_x = \pi$ and b) $k_x = k_y$ with $V_1 = V_2 = V_3 = 1, t = 1, t' = 0.75, t'' = 0.5$ , $t''$ is the diagonal hopping parameter . . .	43
4.35	a)Cross section for the (a) $a_+$ bands and (b) $a_-$ bands in the band structure with parameters $t = 1, t' = 0.75, t'' = 0, g = 0.2, V_1 = V_3 = 0, V_2 = 1$ . . . . .	45
4.36	a)Cross section for the (a) $a_+$ bands and (b) $a_-$ bands in the band structure with parameters $t = 1, t' = 0.75, t'' = -0.5, g = 0.2, V_1 = V_3 = 0, V_2 = 1$ . . . . .	45
4.37	a)Cross section for the (a) $a_+$ bands and (b) $a_-$ bands in the band structure with parameters $t = 1, t' = 0.75, t'' = 0, g = 1, V_1 = V_3 = 0, V_2 = 1$ . . . . .	46
4.38	a)Cross section for the (a) $a_+$ bands and (b) $a_-$ bands in the band structure with parameters $t = 1, t' = 0.75, t'' = -0.5, g = 1, V_1 = V_3 = 0, V_2 = 1$ . . . . .	46
4.39	a)Cross section of the bands with ( $V_1 = V_2 = V_3 = 1, t = 1, t' = 0.75, m = 0.5, g = 0.5$ ) through plane $k_x = \pi$ and b) diagonal plane $k_x = k_y$ . . . . .	47
4.40	a)Cross section of the bands with ( $V_1 = V_3 = 0, V_2 = 1, t = 1, t' = 0.75, m = 0.5, g = 0.5$ ) through plane $k_x = \pi$ and b) diagonal plane $k_x = k_y$ . . . . .	48
4.41	a)Cross section of the bands with ( $V_1 = V_2 = V_3 = 1, t = 1, t' = 0.75, t'' = 0.5, m = 0.3, g = 0.5$ ) through plane $k_x = \pi$ and b) diagonal plane $k_x = k_y$ . Here $t''$ is the diagonal hopping.	48
5.1	a)Band dispersion of the ‘a’ bands in region $[0, 2\pi]$ for staggered case and (b) density of states with $t = 1, V_1 = V_3 = 0, V_2 = 1$ . . . . .	52
5.2	Fermi surface for Von-Hove singularity a)at $\omega = -1.08$ and b) $\omega = 2.0808$ with ( $t = 0.75, V_1 = V_3 = 0, V_2 = 1$ ) . . . . .	53
5.3	Eigenvector for a)the middle band b)lower band c)top band for staggered case case with $t' = 0.75$ and $V_1 = V_3 = 0, V_2 = 1$ .	53
5.4	a)Band dispersion of the ‘a’ bands in region $[0, 2\pi]$ and (b) density of states for symmetric case with $t = 0.75, V_1 = V_2 = V_3 = 1$ . . . . .	54
5.5	Fermi surface for Von-Hove singularity a)at $\omega = -0.5$ and b) $\omega = 2.5$ ( $t = 0.75, V_1 = V_2 = V_3 = 1$ ) . . . . .	54

5.6	Eigenvector for a)the middle band b)lower band c)top band for symmetric case with $t' = 0.75$ and $V_1 = V_2 = V_3 = 1$ . . . . .	55
5.7	a)Band structure for symmetric case for electrons in $a$ orbital with parameters $t = 0.75, t' = 0.6, t'' = -0.5$ , (b)Cross section of the band dispersions in fig(a) for $a$ orbital electrons through plane $k_x = \pi$ . . . . .	56
5.8	Cross section of the band structure for $a$ orbital through the plane $k_x = k_y$ with parameters $t = 0.75, t' = 0.6, t'' = -0.5$ . . . . .	56
5.9	a)DOS for symmetric case for $a$ bands with ( $t = 0.75, t' = 0.6, t'' = -0.5$ ), (b)Number density for symmetric case for $a$ bands for the DOS in fig(a) . . . . .	57
5.10	a)Band structure for staggered case for electrons in $a$ orbital with parameters $V_1 = V_3 = 0, V_2 = 1, t = 0.75, t' = 0.6, t'' = -0.5$ , (b)Cross section of the band dispersions in fig(a) for $a$ orbital electrons through plane $k_x = \pi$ . . . . .	57
5.11	Cross section of the band dispersions for $a$ through the diagonal plane $k_x = k_y$ with parameters $V_1 = V_3 = 0, V_2 = 1, t = 0.75, t' = 0.6, t'' = -0.5$ . . . . .	58
5.12	a)DOS for staggered case for $a$ bands with ( $t = 0.75, t' = 0.6, t'' = -0.5$ ), (b)Number density for staggered case for $a$ bands for the DOS in fig(a) . . . . .	58
5.13	Dispersion relation for symmetric case for $a$ bands with ( $t = 0.75, t' = 0.6, t'' = -0.5$ ) . . . . .	59
5.14	Dispersion relation for symmetric case for $b$ bands with ( $t = 0.75, t' = 0.6, t'' = -0.5$ ) . . . . .	59
5.15	Cross section of the band dispersions for all bands through the plane $k_x = \pi$ with parameters $t = 0.75, t' = 0.6, t'' = -0.5, V_1 = V_2 = V_3 = 1$ . . . . .	59
5.16	Cross section of the band dispersions for all bands through the plane $k_x = k_y$ with parameters $t = 0.75, t' = 0.6, t'' = -0.5, V_1 = V_2 = V_3 = 1$ . . . . .	60
5.17	DOS for the symmetric case with $t=0.75, t'=0.6, t''=-0.5$ . . . . .	60
5.18	Fermi surface for symmetric case for $a$ with ( $t = 0.75, t' = 0.6, t'' = -0.5$ ) for Von-Hove singularity at $\omega = -1.099$ . . . . .	61
5.19	Fermi surface for symmetric case for $a$ with ( $t = 0.75, t' = 0.6, t'' = -0.5$ ) for Von-Hove singularity at $\omega = 0.95683$ . . . . .	61
5.20	Fermi surface for symmetric case for $b$ with ( $t = 0.75, t' = 0.6, t'' = -0.5$ ) for Von-Hove singularity at $\omega = 0.99684$ . . . . .	61
5.21	Fermi surface for symmetric case for $b$ with ( $t = 0.75, t' = 0.6, t'' = -0.5$ ) for Von-Hove singularity at $\omega = 2.0023$ . . . . .	61

5.22	Dispersion relation for symmetric case for $a$ bands with ( $t = 0.75, t' = 0.6, t'' = -0.5$ ) . . . . .	62
5.23	Dispersion relation for staggered case for $b$ bands with ( $t = 0.75, t' = 0.6, t'' = -0.5$ ) . . . . .	62
5.24	Cross section of the band dispersions for all bands through the plane $k_x = \pi$ with parameters $t = 0.75, t' = 0.6, t'' = -0.5, V_1 = V_3 = 0, V_2 = 1$ . . . . .	62
5.25	Cross section of the band dispersions for all bands through the diagonal plane $k_x = k_y$ with parameters $t = 0.75, t' = 0.6, t'' = -0.5, V_1 = V_3 = 0, V_2 = 1$ . . . . .	63
5.26	DOS for the staggered case with $t=0.75, t'=0.6, t''=-0.5$ . . . . .	63
5.27	Fermi surface for staggered case for lower bands with ( $t = 0.75, t' = 0.6, t'' = -0.5$ ) for Von-Hove singularity at $\omega = -1.8182$ . . . . .	64
5.28	Fermi surface for staggered case for lower bands with ( $t = 0.75, t' = 0.6, t'' = -0.5$ ) for Von-Hove singularity at $\omega = -0.0272$ . . . . .	64
5.29	Fermi surface for staggered case for top bands with ( $t = 0.75, t' = 0.6, t'' = -0.5$ ) for Von-Hove singularity at $\omega = -0.00316$ . . . . .	64
5.30	Fermi surface for staggered case for top bands with ( $t = 0.75, t' = 0.6, t'' = -0.5$ ) for Von-Hove singularity at $\omega = 0.99548$ . . . . .	64

# Chapter 1

## Introduction

There has been a consistent search to find materials which shows exotic properties and are of extreme interest. Since the discovery of quantum hall effect in 1980s, there has been a constant search for new topological states of matter. Since then, a tremendous amount of work has been done in this field. The Shastry Sutherland lattice is an example of this. The lattice was predicted theoretically first and few years down the line, it was experimentally found in real materials. Hence, we plan to come up with results which could serve as prescription for experimentalists to look for new materials which can host novel phases. The phases would be already predicted theoretically.

The area of topological insulators has been a very active field in the last decades and still continue to be one. The topological insulators are different from the normal insulators in that the topological insulators behave as an insulator in the bulk but acts as a conductor on the surface because of the presence of gapless surface states. There are certain parameters by which one can check if an insulator is topologically trivial or non-trivial. This quantity is known as the  $Z_2$  invariant[2] [3]. One should keep in mind that the gapless edge survives the effects of weak perturbation. However, this is not true if time reversal symmetry is broken.

In my thesis, I start with a model on a Lieb lattice. A Lieb lattice is a two dimensional section of a perovskite structure and perovskite structure is seen extensively. Then we consider the various phases in the model. We show a Mott metal insulator transition in the model. Then we go to the topological aspect of the band structure. We start with the simplest case with only two hoppings-one inter dimer and another intra dimer hopping. The second chapter deals with the basics of Green's functions at zero temperature and then introduction to Berry phase. In the next section, the methods have

been discussed. To solve the model, DMFT technique has been used. Also the lattice model was mapped to Falicov Kimball impurity model.

The next chapter describes the model along with the results with various hoppings and effects of electric field. We also study the effects of Rashba spin orbit coupling in the system, which arises when the centrosymmetry is broken due to electric field or any other source. The model is also mapped to the Haldane model, which shows that a topological transition is possible.

In the next chapter, we map the model to a two-orbital per site system and we investigate if the features of the dimer model still survives. We want to investigate what happens when the 2D layers are stacked to give a 3D structure.

# Chapter 2

## Theory

### 2.1 Many Body Physics

#### 2.1.1 Green's function

Solving a Hamiltonian is often a difficult task. Most of the times, the total Hamiltonian cannot be solved exactly. Usually, the Hamiltonian is divided into two parts - one which can be exactly solved and other the remaining parts of the Hamiltonian.

$$H = H_0 + V \quad (2.1)$$

where  $H_0$  is the exactly solvable part.  $H_0$  is chosen in a fashion such that the effects of  $V$  are small. For a start,  $H_0$  is solved first and then  $V$  is introduced. We will be using the interaction representation. In interaction representation, both the operator and the state evolves. Let  $O$  and  $\Psi$  be an operator and a state respectively. They evolve as in the following fashion:

$$O(t) = e^{iH_0t} O e^{-iH_0t} \quad (2.2)$$

$$\Psi(t) = e^{iH_0t} e^{-iHt} \Psi(0) \quad (2.3)$$

If we define an evolution operator  $U(t) = e^{iH_0t} e^{-iHt}$  such that  $\Psi(t) = U(t)\Psi(0)$  and assume that  $[H_0, V] \neq 0$  and  $U(0) = 1$ . Differentiating  $U(t)$  with respect to time gives us a differential equation:

$$\frac{\partial}{\partial t} U(t) = -iV(t)U(t) \quad (2.4)$$

$$\implies U(t) = 1 - i \int_0^t dt_1 V(t_1)U(t_1) \quad (2.5)$$

Similarly, we can write an integral equation for  $U(t_1)$  and plug it in the above equation. We can keep on doing that and the finally, we will get a form for

$U(t)$ :

$$U(t) = \sum_{n=0}^{\infty} (-i)^n \int_0^t dt_1 \int_0^{t_1} dt_2 \dots \int_0^{t_{n-1}} dt_n V(t_1) V(t_2) \dots V(t_n) \quad (2.6)$$

If we introduce a time-ordering operator  $T$ , the whole series can be re-written as

$$U(t) = 1 + \sum_0^{\infty} \frac{(-i)^n}{n!} \int_0^t dt_1 \int_0^{t_1} dt_2 \dots \int_0^{t_{n-1}} dt_n T[V(t_1) V(t_2) \dots V(t_n)] \quad (2.7)$$

$$= T \exp \left[ -i \int_0^t dt_1 V(t_1) \right] \quad (2.8)$$

Now we define an operator  $S(t, t')$  called the S matrix which is given by  $\Psi(t) = S(t, t') \Psi(t')$ . It can be shown that the operator can be written as  $S(t, t') = T \exp[-i \int_{t'}^t dt_1 V(t_1)]$  where  $T$  is the time ordering operator. The main motive is to find the ground state of the  $H$ . Let us assume that the exact ground state of  $H_0$  be  $\Psi_0$ . It is assumed that the system is in state  $\Psi_0$  at  $t \rightarrow \infty$  where the effects of interactions are not considered. The system is then adiabatically varied upto time  $t = 0$ .  $\Psi(0)$  is the ground state wavefunction of the system at time  $t=0$  in interaction representation. It has been shown that at zero temperature  $\Psi(0) = S(0, -\infty) \Psi_0$ . At  $t=0$ , the interaction is switched on. The next step is to calculate the Green's function. The electron Green's function in Heisenberg representation is given by

$$G(\eta, t - t') = -i \langle | T c_{\eta}(t) c_{\eta}^{\dagger}(t') | \rangle \quad (2.9)$$

where  $\eta$  can be momentum wave vector or spin and  $T$  is the time ordering operator. The expectation is taken with respect to the ground state of the total Hamiltonian  $H$ . The operators are in interaction representation. We change the state  $| \rangle$  into its interaction representation using the S-matrix.  $| \rangle_0$  is the ground state of the system without any interaction at zero temperature. Using the properties of S-matrix and time operators, the Green's can be written as

$$G(\eta, t - t') = -i \frac{\langle | T \hat{c}_{\eta}(t) \hat{c}_{\eta}^{\dagger}(t') S(\infty, -\infty) | \rangle_0}{\langle | T S(\infty, -\infty) | \rangle_0} \quad (2.10)$$

If there is no interaction, then the free or unperturbed Green's function is

$$G^{(0)}(\eta, t - t') = -i_0 \langle | T \hat{c}_{\eta}(t) \hat{c}_{\eta}^{\dagger}(t') | \rangle_0 \quad (2.11)$$

Similarly, phonon Green's function can be written as

$$D(q, t - t') = i \frac{\langle | T A_q(t) A_{-q} S(\infty, -\infty) | \rangle_0}{\langle | S(\infty, -\infty) | \rangle_0} \quad (2.12)$$



where  $A_q = a_q + a_{-q}$  is the phononic displacement operator. It is possible to have a system where there both electronic and phononic contributions come into the Hamiltonian. In that case, the ground state will be a combination of the ground states for the electrons, phonons. The next step would be to calculate the Green's function. If we expand the S-matrix, the Green's function can be written as a series:

$$G(\eta, t - t') = \sum_{n=0}^{\infty} \frac{(-i)^{n+1}}{n!} \int_{-\infty}^{\infty} dt_1 \dots \int_{-\infty}^{\infty} dt_n \frac{{}_0 \langle | T \hat{c}_\eta \hat{V}(t_1) \hat{V}(t_2) \dots \hat{V}(t_n) \hat{c}_\eta^\dagger(t') | \rangle_0}{{}_0 \langle | S(\infty, -\infty) | \rangle_0} \quad (2.13)$$

In order to evaluate the time ordered expectation of the brackets  ${}_0 \langle | T \hat{c}_\eta \hat{V}(t_1) \hat{V}(t_2) \dots \hat{V}(t_n) \hat{c}_\eta^\dagger(t') | \rangle_0$ , we will need to understand how to pair the operators. The following rules should be followed:

- When we pair the operators, there should be equal number of creation and annihilation operator. Mathematically, it can be thought that the action of a annihilation operator on a  $\langle |$  is equivalent to action of a creation operator on a  $| \rangle$  or vice versa. So, if there are unequal number of creation and annihilation operators, then the final *bra* and *ket* would be orthogonal and hence the expectation would be zero. Physically, this is to ensure the particle number is conserved.
- For a The operators should have the same index. Let us take the take the example of a fermionic creation operator  $c_\alpha^\dagger$  which when acted upon  $| \rangle_0$  creates an electron in the  $\alpha$  state. Now before the action of  $\langle |_0$ , it must be acted upon by a lowering operator to have a non-zero expectation. Now, the point is the lowering operator should have the same  $\alpha$  i.e.  $c_\alpha$  will act. Then, the expectation will be finite.
- All possible pairings of creation and annihilation operator should be considered. Also each pair should be time ordered. Let us consider the following example:

$$\begin{aligned} & {}_0 \langle | T \hat{c}_\alpha(t) \hat{c}_\beta^\dagger(t_1) \hat{c}_\gamma(t_2) \hat{c}_\delta^\dagger(t') | \rangle_0 \\ & = {}_0 \langle | T \hat{c}_\alpha(t) \hat{c}_\beta^\dagger(t_1) | \rangle_{00} \langle | T \hat{c}_\gamma(t_2) \hat{c}_\delta^\dagger(t') | \rangle_0 \\ & - {}_0 \langle | T \hat{c}_\alpha(t) \hat{c}_\delta^\dagger(t') | \rangle_{00} \langle | T \hat{c}_\gamma(t_2) \hat{c}_\beta^\dagger(t_1) | \rangle_0 \end{aligned} \quad (2.14)$$

This is known as the Wick's theorem. If there are  $n$  creation and destruction operators, there are  $n!$  ways possible to pair them. There is a negative sign in front of the second term. This is because when two fermionic operators are interchanged, it picks up a negative sign. So, if there are odd number of interchanges, there will be a negative sign.

- In order to pair a term having a combination of different kinds of operators, each type of operator is paired separately. This is because the electron operators will commute with the phonon operators.

$${}_0 \langle | T \hat{c}_k(t) \hat{c}_{k_1}^\dagger(t_1) \hat{A}_{q_1}(t_2) \hat{c}_{k_2}(t_3) \hat{c}_{k_3}^\dagger(t_4) \hat{A}_{q_2}(t') | \rangle_0 = {}_0 \langle | T \hat{c}_k(t) \hat{c}_{k_1}^\dagger(t_1) \hat{c}_{k_2}(t_3) \hat{c}_{k_3}^\dagger(t_4) | \rangle_{00} \langle | T \hat{A}_{q_1}(t_2) \hat{A}_{q_2}(t') | \rangle_0 \quad (2.15)$$

So the electron operators will be paired further independently of the phonon operators. The Wick theorem will be applied to both the operators.

- If both the operators act at the same time, then the ordering of the operators is as follows:

$${}_0 \langle | T \hat{c}_{k_1}^\dagger(t_1) \hat{c}_{k_2}(t_2) | \rangle_0 = \delta_{k_1=k_2} {}_0 \langle | \hat{c}_{k_1}^\dagger(t_1) \hat{c}_{k_2}(t_2) | \rangle_0 = \delta_{k_1=k_2} n_f(\varepsilon_{k_1}) \quad (2.16)$$

where  $n_F$  is the fermionic number operator. If they are at different times, the creation operator is put to the right.

So, it can be seen that each term in the expansion will either be a Green's function or a number operator. So if we have only  $V(t_1)$ , it is the first order interaction. We can have higher order interactions in the Green's function calculation where we consider  $V(t_1) \dots V(t_n)$ .

## 2.1.2 Feynman Diagrams

Expanding the series representation of Green's function will yield many terms with more number of operators and hence it becomes very difficult to keep track of the terms. So, it is useful to represent the terms using Feynman diagrams. It also helps us to keep the terms which contribute to the actual physical process and discard the rest. The electron Green's function is represented by a line with momentum written on it and an arrow is put on the line to indicate the direction of time flow. Similarly, for the phonon case, the line is now replaced by dotted line. Here, there is no arrow. The number operator is represented by a loop. This is because both the operators are at

same time, so it has to close back to itself.

A diagram with a single electron line and single phonon line will represent a electron phonon interaction. At each vertex, the total incoming momentum will be equal to total outgoing momentum. Now one important thing to note is that a diagram can either be connected or disconnected. The disconnected diagrams are those which can be separated into two distinct parts without making a cut.

The next thing is to evaluate the expectation  ${}_0 \langle | S(\infty, -\infty) | \rangle_0$ . This can be written as a series given by

$${}_0 \langle | S(\infty, -\infty) | \rangle_0 = \sum_{n=0}^{\infty} \frac{(-i)^n}{n!} \int_{-\infty}^{\infty} dt_1 \dots \int_{-\infty}^{\infty} dt_n \times {}_0 \langle | TV(t_1)V(t_2)\dots V(t_n) | \rangle_0 \quad (2.17)$$

This term will also give rise to terms known as vacuum polarization terms. So, it would be tedious to first find the diagrams for the numerator in the expansion for Green's function and then the vacuum polarization. However, there is a theorem which simplifies the calculation. According to the theorem, the disconnected diagrams in the expansion of the term in the numerator gets cancelled by the vacuum polarization diagrams in the denominator. Hence, only the contributions from the connected diagrams are included to calculate the Green's function.

### 2.1.3 Dyson's Equation

Interacting Green's function include self energy terms which is basically the energy change because of interaction. It is often easier to work in the Fourier domain(energy) while calculating. The Fourier transform is given by:

$$G(p, E) = \int_{-\infty}^{\infty} dt e^{iE(t-t')} G(p, t - t') \quad (2.18)$$

Similarly, for a phonon, the frequency domain Green's function is defined as

$$D(q, \omega) = \int_{-\infty}^{\infty} dt e^{i\omega t} D(q, t) \quad (2.19)$$

Upon calculating the various terms in the expansion, we get the final interacting Green's function as [4]

$$G(p, E) = G^{(0)}(p, E) + G^{(0)}(p, E)^2 \Sigma^{(1)}(p, E) + \dots \quad (2.20)$$

where  $G^{(0)}(p, E)$  is the unperturbed Green's function and  $\Sigma^{(1)}(p, E)$  is the first order self energy. There will be other higher terms having higher order

self-energies. Finally incorporating all the terms, it can be shown that,

$$G(p, E) = \frac{G^{(0)}(p, E)}{1 - G^{(0)}(p, E)\Sigma(p, E)} \quad (2.21)$$

where  $\Sigma(p, E)$  is the total self-energy, calculated by summing all the self-energies. This is known as the Dyson's equation. So, if we know both interacting and non-interacting Green's function, then self-energy can be calculated using this equation. Everything we have considered was for zero temperature. At non-zero temperatures, the expectation value is calculated by averaging over all the possible configurations. For non-zero temperatures, Matsubara Green's function are defined which works in complex plane. From, Matsubara Green's function, the retarded Green's function is obtained by analytic continuation.

## 2.2 Band Topology

Let us now look at the topological aspect of the band structure. As we know in topology, continuous deformation changes the shape of an object, however, keeps the genus conserved. In physics, the continuous deformation is equivalent to adiabatic continuity. Let us consider a system having a ground state and an excited state with an energy difference  $\Delta E$  between them. By adiabatic continuity it is meant that if the Hamiltonian is varied slowly, the two levels don't cross each other. The time scale of varying the Hamiltonian is much less than that determined by the uncertainty principle ( $t \ll \frac{\hbar}{\Delta E}$ ). So two states will be same topologically, if they can be connected adiabatically to each other. To understand the band topology, it is first required to understand what the Berry phase is and what it implies.

### 2.2.1 Berry Phase

The concept of Berry phase was first introduced in 1983[5]. Let us consider a Hamiltonian which depends on some parameter  $R$ . The Hamiltonian is varied adiabatically by varying the parameter. The wavefunction of the system acquires a phase, other than the phase dictated by time evolution. This geometric phase is known as the Berry phase.

Let  $|\Psi(t)\rangle$  be the wavefunction of the system at time  $t$ . It evolves as

$$i\hbar \frac{\partial |\Psi(t)\rangle}{\partial t} = \hat{H}(R)|\Psi(t)\rangle \quad (2.22)$$

$$\hat{H}(R)|n(R)\rangle = E_n|n(R)\rangle \quad (2.23)$$

$|n(R)\rangle$  form a basis at each instant. So, if a system is prepared in one of the eigen states, say  $|n(R(0)\rangle$ , the wavefunction of the system at any instant will be given by

$$|\Psi(t)\rangle = \exp\left\{-\frac{i}{\hbar} \int_0^t dt' E_n(R(t'))\right\} \exp\{i\gamma_n(t)\} |n(R(t))\rangle \quad (2.24)$$

The first exponential corresponds to the phase factor due to time evolution and the second is the factor due to geometric phase. We plug this in the time dependent Schrodinger wave equation. We get the LHS as

$$\begin{aligned} i\hbar \frac{\partial |\Psi(t)\rangle}{\partial t} &= i\hbar \left[ \frac{-i}{\hbar} E_n(R(t)) \exp\{i\gamma_n(t)\} |n(R(t))\rangle + i\dot{\gamma}_n(t) \exp\{i\gamma_n(t)\} |n(R(t))\rangle \right. \\ &\quad \left. + \exp\{i\gamma_n(t)\} \frac{\partial |n(R(t))\rangle}{\partial t} \right] \exp\left\{-\frac{i}{\hbar} \int_0^t dt' E_n(R(t'))\right\} \end{aligned} \quad (2.25)$$

The RHS reads as

$$\hat{H} |\Psi(t)\rangle = E_n \exp\left\{-\frac{i}{\hbar} \int_0^t dt' E_n(R(t'))\right\} \exp\{i\gamma_n(t)\} |n(R(t))\rangle \quad (2.26)$$

Upon equating the two, we get

$$\dot{\gamma}_n(t) |n(R(t))\rangle = i \frac{\partial}{\partial t} |n(R(t))\rangle \quad (2.27)$$

$$\implies \dot{\gamma}_n(t) = i \langle n(R(t)) | \nabla_R n(R(t)) \rangle \cdot \dot{R}(t) \quad (2.28)$$

Over a circuit, i.e.  $R(0)=R(t)$ , we will have

$$\gamma_n(C) = i \oint_C \langle n(R(t)) | \nabla_R n(R(t)) \rangle \cdot dR \quad (2.29)$$

We will now show that  $\gamma_n(C)$  is real. Orthonormality guarantees

$$\langle n(R) | n(R) \rangle = 1 \quad (2.30)$$

$$\implies \nabla_R \langle n(R) | n(R) \rangle = 0 \quad (2.31)$$

$$\implies \langle \nabla_R n(R) | n(R) \rangle + \langle n(R) | \nabla_R n(R) \rangle = 0 \quad (2.32)$$

$$\implies (\langle n(R) | \nabla_R n(R) \rangle)^* + \langle n(R) | \nabla_R n(R) \rangle = 0 \quad (2.33)$$

$$\implies 2\text{Re}(\langle n(R) | \nabla_R n(R) \rangle) = 0 \quad (2.34)$$

Hence,  $\gamma$  is imaginary. Using Stokes theorem,

$$\begin{aligned}\gamma_n(C) &= -Im \int \int dS. \nabla \times \langle n | \nabla n \rangle \\ &= -Im \int \int dS. \langle \nabla n | \times | \nabla n \rangle + Im \int \int dS. \times \langle n | \nabla \times | \nabla n \rangle\end{aligned}\quad (2.35)$$

The second term goes to zero. Therefore, expanding this in terms of eigen basis  $[|m(R)\rangle]$ , we get

$$\gamma_n(C) = -Im \int \int_C dS. \sum_{m \neq n} \langle \nabla n | m \rangle \times \langle m | \nabla n \rangle \quad (2.36)$$

We need to evaluate these terms.

$$H|n\rangle = E_n|n\rangle \quad (2.37)$$

$$\implies \nabla(H|n\rangle) = \nabla E_n|n\rangle \quad (2.38)$$

$$\implies \nabla H|n\rangle + H\nabla|n\rangle = E_n\nabla|n\rangle \quad (2.39)$$

$$\implies \langle m | \nabla H | n \rangle + \langle m | H (\nabla H | n \rangle) = E_n \langle m | \nabla n \rangle \quad (2.40)$$

$$\implies \langle m | \nabla H | n \rangle = (E_m - E_n) \langle m | \nabla n \rangle \quad (2.41)$$

Let us define

$$V_n(R) = Im \sum_{m \neq n} \frac{\langle n | \nabla H | m \rangle \times \langle m | \nabla H | n \rangle}{(E_m - E_n)^2} dS \quad (2.42)$$

$$\gamma_n(C) = - \int \int_C dS. V_n(R) \quad (2.43)$$

Similar to magnetic field,  $V_n$  is a curl of a vector. So,  $V_n(R)$  can be thought as a magnetic field.

Let us consider system having two states + and -. which has energy  $E_+$  and  $E_-$  respectively. Let the system has a degeneracy at some point  $R^*$  i.e.  $E_+(R^*) = E_-(R^*)$ .

Expanding the Hamiltonian near the degeneracy ( $R$  is very close to  $R^*$ ), we get the Hamiltonian upto first order as

$$H(R) = H(R^*) + \nabla H(R^*)(R - R^*) \quad (2.44)$$

Differentiating both sides with respect to  $R$ ,

$$\nabla H(R) = \nabla H(R^*) \quad (2.45)$$

Therefore, using equation(21)

$$V_+(R) = Im \frac{\langle + (R) | \nabla H(R^*) | - (R) \rangle \times \langle - R | \nabla H(R^*) | + R \rangle}{(E_+(R) - E_-(R))^2} \quad (2.46)$$

In order to evaluate  $V_+(R)$ . Let us assume that the point of degeneracy is  $R^* = 0$  and  $E_{\pm} = 0$ . A spin- $\frac{1}{2}$  Hamiltonian can be represented by  $2 \times 2$  matrix and we know that the Pauli matrices span the space of all  $2 \times 2$  matrices. So we can write the Hamiltonian in terms of Pauli matrices. Let us define:

$$|+\rangle = \begin{bmatrix} 1 \\ 0 \end{bmatrix}, |-\rangle = \begin{bmatrix} 0 \\ 1 \end{bmatrix}$$

Therefore, at some point  $R$  in parameter space, we can have

$$\sigma_x |\pm\rangle = |\mp\rangle, \sigma_y |\pm\rangle = \pm i |\mp\rangle, \sigma_z |\pm\rangle = |\pm\rangle \quad (2.47)$$

where the  $\sigma_x, \sigma_y, \sigma_z$  are the Pauli spin matrices. This is true only when the spin points towards the field and if we vary the field slowly, this can be achieved. Using this assumption, we have

$$V_{x+} = Im \frac{\langle + | \sigma_y | - \rangle \langle - | \sigma_z | + \rangle}{2R^2} = 0 \quad (2.48)$$

$$V_{y+} = Im \frac{\langle + | \sigma_z | - \rangle \langle - | \sigma_x | + \rangle}{2R^2} = 0 \quad (2.49)$$

$$V_{z+} = Im \frac{\langle + | \sigma_x | - \rangle \langle - | \sigma_y | + \rangle}{2R^2} = \frac{1}{2R^2} \quad (2.50)$$

Plugging this into the main equation, we get

$$V_+(R) = \frac{\mathbf{R}}{2R^3} \quad (2.51)$$

Now the field has a singularity at  $R = 0$ , which is the point of degeneracy. Therefore, any  $C$  enclosing the degeneracy will have a non-zero phase.

$$\gamma_n(C) = - \int \int_C dS \cdot \frac{\mathbf{R}}{R^3} = -\frac{1}{2} \Omega(C) \quad (2.52)$$

. This can be thought as the solid angle viewed from the point of degeneracy. Also, in analogy with Gauss's law, it can be viewed as the magnetic flux through loop  $C$  because of a pseudo magnetic charge at the degeneracy[5].

# Chapter 3

## Methods

### 3.1 Dynamical Mean Field Theory

Mean field theories are extensively used for solving a many body Hamiltonian. It is difficult to solve the many body Hamiltonian exactly for a large number of particles because of very high number of degrees of freedom. So, by using mean field approximation, the degrees of freedom can be reduced. If we have a particle, the mean field approximation gives us the average field due to all other particles in the system at that point. In this way, instead of having individual terms and their interactions, by considering an average field we can reduce the number of degrees and hence simplify the problem.

There are many mean field theories. Each uses some different sets of approximations. However, the basic tenet behind each of them is still the same. In order to solve our problem, dynamical mean field theory has been used. Quantum mechanical many body systems are difficult to solve in finite dimensions because of the complicated algebra involved. We know that even the same holds for classical models. The Weiss molecular field theory becomes exact as  $Z \rightarrow \infty$ . Dynamical mean field theory usually maps the problem to models which are exact in the limit of infinite dimensions.

#### 3.1.1 Motivations for using infinite dimensions

If the system under consideration is a perfect crystalline, then each lattice point will have the same number of neighbours, which is called the coordination number, often denoted by the symbol 'Z'. If we look at three dimensional simple cubic lattice(d=3), the number of nearest neighbours is  $Z=6$ . If we expand  $\frac{1}{Z}$ , we can see that the higher order terms goes as  $\frac{1}{6}, \frac{1}{36}$  and becomes negligible. So the higher order terms don't contribute significantly as compared to the lower order. They decay faster. So the problem can be extended



to infinite dimensions where it becomes exact and only the zeroth order term contributes.

### 3.1.2 Classical Spin Model

Before moving to the dynamical mean field theory, it is important to know the classical spin model and the effect of dimensions on it. If we consider the classical Heisenberg model, the Hamiltonian of which is given by

$$H = -\frac{1}{2}J \sum_{\langle ij \rangle} S_i S_j \quad (3.1)$$

where  $J$  is the coupling and  $S_i$  is the spin. The sum is over nearest neighbours and the factor of  $\frac{1}{2}$  is introduced to avoid double counting. To solve the model, mean field approximation is used. The aim would be to obtain the thermal average of magnetization,  $m_i = \langle S_i \rangle$ . The effective Hamiltonian becomes an interaction between the spin and an average ("molecular") field. So the mean field Hamiltonian is

$$H_M = -H_w \sum_i S_i + \text{constant} \quad (3.2)$$

where  $H_w = J \sum_j \langle S_j \rangle$ . Here the correlated spin fluctuations at different sites have been neglected. If the coordination number  $Z$  is very large i.e. the limit  $Z \rightarrow \infty$ , then the  $H_w$  will not be finite. So, the  $J$  needs to be rescaled as  $J \rightarrow \frac{J}{Z}$ . In the limit  $Z \rightarrow \infty$ , the spin fluctuations can be neglected and the total Hamiltonian can be replaced by a local one and it becomes a single site problem which is easier to solve.

### 3.1.3 Hubbard model in high dimensions

The next thing would be to know the effects of dimensionality on quantum mechanical lattice models. The single orbital spin- $\frac{1}{2}$  Hubbard model on a  $D$  dimensional cubic lattice is given by,

$$H = \frac{t}{\sqrt{2D}} \sum_{\langle ij \rangle, \sigma} c_{i\sigma}^\dagger c_{j\sigma} + U \sum_i n_{i\uparrow} n_{i\downarrow} \quad (3.3)$$

The first term in the Hamiltonian is the kinetic energy and the second is the interaction term. The parameters in the Hamiltonian are scaled to obtain a non-trivial density of states and a finite kinetic energy (cite the paper by Metzner and Volhardt) as  $D \rightarrow \infty$ . Considering nearest neighbor hopping, the kinetic energy can be written in the momentum space as

$$H_{kin} = \sum_{k,\sigma} \varepsilon(k) c_{k,\sigma}^\dagger c_{k,\sigma} \quad (3.4)$$

$$\varepsilon(k) = \frac{2t}{\sqrt{2D}} \sum_{n=1}^D \cos(k_n) \quad (3.5)$$

The density of states for the system is given by

$$\rho(\varepsilon) = \sum_k \delta(\varepsilon - \varepsilon(k)) \quad (3.6)$$

The density of states sum is nothing but the probability density of an event  $\varepsilon = \varepsilon_k$ . Also  $k_i$  are chosen randomly from  $k_1, \dots, k_D$ . It has been shown that in the limit of infinite dimensions the non-interacting density of states tends to a Gaussian distribution in infinite dimensions[6].

$$\rho(\varepsilon) \rightarrow \exp\{-\varepsilon^2/2t^2\}/\sqrt{2\pi t^2} (D \rightarrow \infty) \quad (3.7)$$

This result directly follows from the central limit theorem. Since  $k_i$ s are chosen randomly,  $\varepsilon_k$  is the sum of random numbers. Also the  $k_i$ s are independent of each other. Therefore, in the limit of infinite dimensions, the distribution should be a Gaussian.

Now the interaction gives rise to self energy terms. Each internal line in the irreducible self energy diagram contributes in  $\mathcal{O}(\frac{1}{\sqrt{d}})$ . However each site has  $2d$  neighbouring sites i.e. each of them contribute in  $\mathcal{O}(d)$ . Now if the number number of vertices is less than twice the number of internal lines, then the diagram doesn't contribute towards the self energy in the limit  $d \rightarrow \infty$ . So only the diagrams at a single site contribute to the self energy term i.e. the field is local[7]. Momentum conservation is no longer needed for individual vertices. However, it is dynamical in time. Consider a single site. If we look at it for a long time, we will find that the spin of the electron at that site keeps on changing. This is because of hopping. As electrons with different spins hop from one site to another, the spin at the local site keeps on changing, hence, dynamical. So the self energy would be a function of time not space. In the fourier space, the self energy would be independent of momentum. However, the momentum would be reflected in the total Green's function in the band energy. We would be using DMFT approximation to solve our model.

## 3.2 Equation of Motion for Green's function

The other way to obtain a Green's function is using the equations of motion developed by Zubarev [8]. Let us consider operators  $A(t)$  and  $B(t)$ . The equation of motion ( $\hbar = 1$ ) for the Green's function  $\langle\langle A(t); B(t') \rangle\rangle$  is

$$i \frac{d}{dt} \langle\langle A; B \rangle\rangle = \frac{d}{dt} \theta(t-t') \langle [A(t), B(t')] \rangle + \langle\langle i \frac{dA(t)}{dt}; B(t') \rangle\rangle \quad (3.8)$$

where  $\theta$  is the heavside function. The second term on the right side of the equation will be equal to  $\langle\langle [A(t), H(t)]; B(t') \rangle\rangle$ . So, this is a higher order Green's function. Similarly, an equation of motion will be written for the higher order Green's function and so on. A chain of equations will be formed. In some cases, the sets of equation acquires a closed form. In those cases, we get the exact Green's function. In other cases, the higher order Green's function is decoupled to close the set of equations. The decoupling is usually done considering some physical process in some limits. After decoupling, the averages of the decoupled terms are calculated self-consistently. Lacroix used a decoupling scheme to solve the Anderson model using the equations of motion and obtained the Kondo resonance[9]. This method have been in use since a long time [10].

## 3.3 Falicov-Kimball Model

In order to solve a lattice Hamiltonian, it is often mapped to an impurity problem. The Falicov Kimball model is basically a single site impurity model. It is a spinless model i.e. the model has two species of spinless electrons. It is assumed that one of the species doesn't hop. The conduction electron hops.

$$H = -t \sum_{\langle ij \rangle} (c_i^\dagger c_j + h.c) + U \sum_i n_{ic} n_{id} \quad (3.9)$$

where  $n_{ic}$  and  $n_{id}$  is the number operator for conduction and localized electrons respectively. Since,  $n_{id} = [0,1]$ , we can write  $v_i = U n_{id} = [0, U]$ .  $v_i$  follows a binary alloy distribution the probability distribution of which is given by  $P(v_i) = (1-x)\delta(v_i) + x\delta(v_i - U)$ . For a symmetric case,  $x = \langle n_{id} \rangle = \frac{1}{2} = \langle n_{ic} \rangle$ .

$$H_{imp} = \sum_k \varepsilon_k c_k^\dagger c_k + \sum_k t_k (c_i^\dagger c_k + h.c) + U n_{ic} n_{id} \quad (3.10)$$

where  $c_k^\dagger (c_k)$  is the creation(annihilation) operator for the bath or conduction electrons. The last term is the on-site repulsion between the conduction and

the impurity electrons. To understand the dynamics of the model, we have to calculate the Green's function. We will be using the equation of motion for the Green's function which was first developed by Zubarev [8]. Equation of motion for the on-site diagonal impurity Green's function is given by

$$\omega G_{ii} = 1 + \sum_k t_k \langle c_k, c_d^\dagger \rangle + U \langle n_{id} c_k; c_i^\dagger \rangle \quad (3.11)$$

where  $G_{ii} = \langle c_i; c_i^\dagger \rangle$  is the Fourier transform of the Green's function in time domain.

$$(\omega - U) \langle n_{id} c_k; c_i^\dagger \rangle = \langle n_{id} \rangle + \sum_k t_k \langle n_{id} c_k; c_i^\dagger \rangle \quad (3.12)$$

$$(\omega - \varepsilon_k) \langle c_k; c_i^\dagger \rangle = t_k G_{ii} \quad (3.13)$$

$$(\omega - \varepsilon_k) \langle n_{id} c_k; c_i^\dagger \rangle = t_k \langle n_{id} c_i; c_i^\dagger \rangle \quad (3.14)$$

These four equations are in a closed form. Solving them we get the the on-site Green's function as

$$G_{ii}(\omega) = \frac{1 - \langle n_{id} \rangle}{\omega - \Delta(\omega)} + \frac{\langle n_{id} \rangle}{\omega - U - \Delta(\omega)} \quad (3.15)$$

where  $\Delta(\omega) = \sum_k \frac{t_k^2}{\omega - \varepsilon_k}$ . This is called the bath function. However, self consistency in bath demands  $\varepsilon_k \rightarrow \varepsilon_k + \Sigma(\omega)$ . So,  $\Delta(\omega) = \sum_k \frac{t_k^2}{\omega - \varepsilon_k - \Sigma(\omega)}$ . The self energy is independent of momentum in infinite dimensions. Its a function of frequency only. For the Bethe lattice,  $\Delta(\omega) = t^2 G_{ii}(\omega)$ .

### 3.4 Metal-insulator transition

To study the metal-insulator transition in the system, we have to find the interacting density of states. The interacting density of states is related to the imaginary part of the Green's function by

$$\rho_{int}(\omega) = -\frac{1}{\pi} \text{Im}g(G(\omega)) \quad (3.16)$$

The green's function has to be calculated self consistently. The algorithm to get the interacting Green's function is given here.

- For a start, we have to consider some value of  $G_0$ . The then the bath function has to be calculated using the formulae

$$G_0 = \frac{1}{\omega + \mu - \Delta(\omega)} \quad (3.17)$$

- Once we get the bath function, we have to calculate the impurity Green's function. The impurity Green's function can be calculated using[11][12]

$$G(\omega) = \frac{w_o}{(\omega + \mu - \Delta(\omega))} + \frac{w_1}{(\omega + \mu - U - \Delta(\omega))} \quad (3.18)$$

where  $w_o + w_1 = 1$ .  $w_1$  can be thought as the probability that the site is occupied by an impurity electron. Since we are considering the symmetric case in our problem, the numerators are both equal to 0.5.

- Using Dyson's equation,we can get the self energy from the impurity Green's function and  $G_0$ .

$$\Sigma(\omega) = \left(\frac{U}{2} - \frac{1}{2G(\omega)}\right) \pm \sqrt{\left(\frac{1}{2G(\omega)} - \frac{U}{2}\right)^2 + \frac{1}{2} \frac{U}{G(\omega)}} \quad (3.19)$$

As it is evident from the above relation, the self energy can have two values because the square root dependence. We choose that branch of the self energy which gives us positive density of states since negative density of states doesn't make sense.

- The next step is to calculate the lattice Green's function

$$G_{lattice} = \frac{1}{N} \sum_k \frac{1}{\omega + \mu - \varepsilon(k) - \Sigma(\omega)} \quad (3.20)$$

- Self consistency demands that the impurity Green's function should be equal to the lattice Green's function.Hence, we set  $G_{lattice} = G(\omega)$ .
- After this, we will update the value of  $G_0$  from  $G(\omega)$  using the Dyson-equation discussed in Chapter 2.
- This loop has to continued until convergence is reached. By convergence, it is meant that the value of lattice Green's function equals that of the impurity Green's function

This method has been used to solve various models [13]. Once the Green's function is obtained, the interacting density of states can be easily obtained. The metal insulator transition can be shown by varying U and its effect on the density of states.

# Chapter 4

## 4.1 Model

The model consists of a Lieb lattice. On each lattice point, we place a dimer. The dimers are arranged in such a fashion that two adjacent dimers are perpendicular to each other and the atoms of one dimer are equidistant from the two atoms of the adjacent dimer. The Lieb lattice has a unit cell having three sites. Let us name them as 1, 2 and 3. On each of them, we place a dimer having two atoms labelled by indices a and b. The Hamiltonian for the model will have terms for intra-dimer as well as inter-dimer hopping apart from the onsite energies.

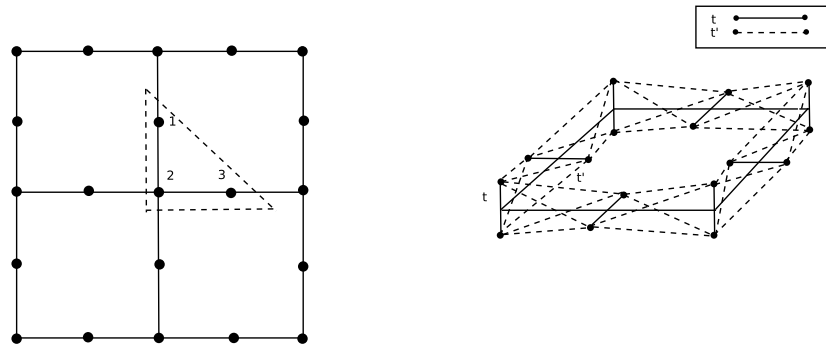


Figure 4.1: Lieb lattice and the model with intra dimer and one inter dimer hopping

The total Hamiltonian for the model can be written as

$$H_{total} = H_{intra} + H_{inter} + H_{on-site} \quad (4.1)$$

The intra-dimer hopping is captured in the Hamiltonian as

$$H_{intra} = -t \sum_i (c_{ia1}^\dagger c_{ib1} + c_{ia2}^\dagger c_{ib2} + c_{ia3}^\dagger c_{ib3}) + h.c. \quad (4.2)$$

where  $c_{ia1}^\dagger$  refers to the creation operator of the atom 'a' of 1st the dimer at  $i$ th unit cell and  $t$  is the hopping parameter. The inter-dimer hopping Hamiltonian for the lattice will be given by

$$\begin{aligned} H_{inter} &= -t' \sum_i (c_{ia1}^\dagger c_{ia2} + c_{ia1}^\dagger c_{ib2}) + h.c - t' \sum_i (c_{ib1}^\dagger c_{ia2} + c_{ib1}^\dagger c_{ib2}) + h.c. \\ &\quad - t' \sum_i (c_{ia3}^\dagger c_{ia2} + c_{ia3}^\dagger c_{ib2}) + h.c - t' \sum_i (c_{ib3}^\dagger c_{ia2} + c_{ib3}^\dagger c_{ib2}) + h.c. \\ &\quad - t' \sum_i (c_{ia1}^\dagger c_{(i+1)a2} + c_{ia1}^\dagger c_{(i+1)b2}) + h.c - t' \sum_i (c_{ib1}^\dagger c_{(i+1)a2} + c_{ib1}^\dagger c_{(i+1)b2}) + h.c. \\ &\quad - t' \sum_i (c_{ia3}^\dagger c_{(i+1)a2} + c_{ia3}^\dagger c_{(i+1)b2}) + h.c - t' \sum_i (c_{ib3}^\dagger c_{(i+1)a2} + c_{ib3}^\dagger c_{(i+1)b2}) + h.c. \end{aligned}$$

If we make a dimer transformation of the form  $a_+ = \frac{1}{\sqrt{2}}(c_a + c_b)$  and  $a_- = \frac{1}{\sqrt{2}}(c_a - c_b)$  with respect to bond axis.

$$\begin{aligned} c_{ia1}^\dagger c_{ib1} &= \left( \frac{a_{+i1}^\dagger + a_{-i1}^\dagger}{\sqrt{2}} \right) \left( \frac{a_{+i1} - a_{-i1}}{\sqrt{2}} \right) \\ &= \frac{1}{2} (a_{+i1}^\dagger a_{+i1} + a_{-i1}^\dagger a_{+i1} - a_{+i1}^\dagger a_{-i1} - a_{-i1}^\dagger a_{-i1}) \\ c_{ib1}^\dagger c_{ia1} &= \frac{1}{2} (a_{+i1}^\dagger a_{+i1} + a_{+i1}^\dagger a_{-i1} - a_{-i1}^\dagger a_{+i1} - a_{-i1}^\dagger a_{-i1}) \end{aligned}$$

The terms can be re-written as

$$-t \sum_i (c_{ia1}^\dagger c_{ib1}) + h.c. = -t \sum_i (a_{+i1}^\dagger a_{+i1} - a_{-i1}^\dagger a_{-i1}) = -t \sum_i (n_{a_{+i1}} - n_{a_{-i1}}) \quad (4.3)$$

Using this, we get the intra-dimer Hamiltonian as

$$H_{intra} = -t \sum_i (n_{a_{+i1}} - n_{a_{-i1}}) - t \sum_i (n_{a_{+i2}} - n_{a_{-i2}}) - t \sum_i (n_{a_{+i3}} - n_{a_{-i3}}) \quad (4.4)$$

Similarly, we can get the inter-dimer Hamiltonian as

$$H_{inter} = -2t' \sum_i (a_{+i1}^\dagger a_{+i2} + a_{+i2}^\dagger a_{+i3} + a_{+i1}^\dagger a_{+(i+1)2} + a_{+i3}^\dagger a_{+(i+1)2}) + h.c. \quad (4.5)$$

So, now the final Hamiltonian in the can be written as

$$H = -2t' \sum_{\langle ij \rangle} (a_{+i}^\dagger a_{+j} + h.c.) + (V-t) \sum_i n_{+i} + (V+t) \sum_i n_{-i} + U \sum_i n_{+i} n_{-i} \quad (4.6)$$

If we consider that the Hamiltonian with intra-dimer and one inter-dimer hopping, we can see that only the  $a_+$  electron hops from one site to another while  $a_-$  doesn't. However, there is an onsite interaction between the  $a_+$  and  $a_-$  electron. So, it can be mapped to the Falicov-Kimball model as discussed in the previous chapter. A Mott transition is expected in this case. When  $t = t'$ , the dispersionless  $a_-$  band is exactly at the Von-Hove singularity of the lower  $a_-$  band. When  $\langle n_+ \rangle = \langle n_- \rangle = 0.5$ , we get the results as

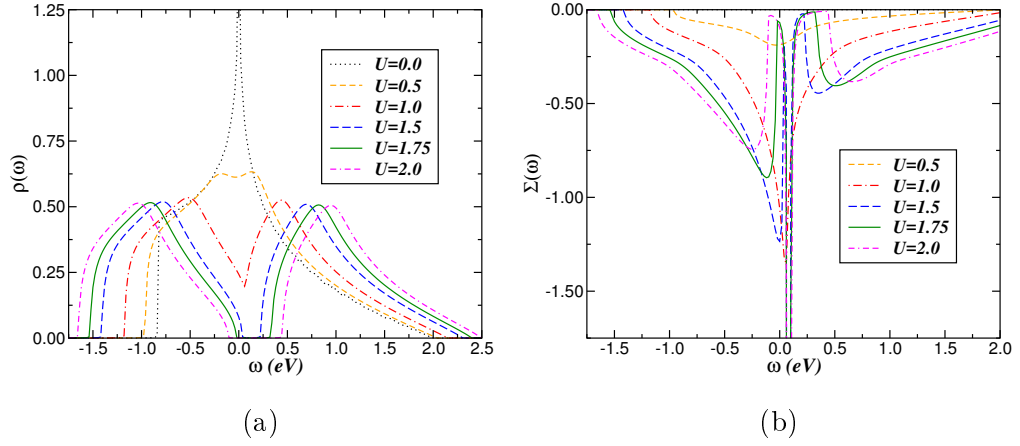


Figure 4.2: a)Mott-transition in the DOS b)Self energy for parameters  $t = t'$  [1]

All the inter-dimer hopping strengths are same here because of the translation symmetry. Using the tight binding approximation, the terms can be written in the momentum space as

$$a_{+i1}^\dagger a_{+i2} = -2t' \sum_k a_{+k1}^\dagger a_{+k2} e^{\frac{ik_y m}{2}}$$

So, the tight binding Hamiltonian for the non-interacting case can be written as

$$\mathcal{H}_0(k) = \sum_k \Phi_k^\dagger H(k) \Phi_k \quad (4.7)$$

where  $\Phi_k = (a_{+1k}, a_{+2k}, a_{+3k}, a_{-1k}, a_{-2k}, a_{-3k})$  is the spinor,  $a_{+1k}$  refers to the creation operator for an electron of  $+$  species at site 1 in the unit cell of the



lattice.  $k$  is the two dimensional momentum. Since, the  $a_-$  electrons are dispersionless, we can consider only the  $a_+$  electrons for now. So the tight binding Hamiltonian matrix for the  $a_+$  in momentum space can be written as

$$H(k) = \begin{bmatrix} V_1 - t & -4t' \cos\left(\frac{k_y}{2}\right) & 0 \\ -4t' \cos\left(\frac{k_y}{2}\right) & V_2 - t & -4t' \cos\left(\frac{k_x}{2}\right) \\ 0 & -4t' \cos\left(\frac{k_x}{2}\right) & V_3 - t \end{bmatrix} \quad (4.8)$$

When all the on-site energies are equal  $V_1 = V_2 = V_3$ , we call it the symmetric case. For the symmetric case, we have the energy eigenvalues as

$$E_1 = V - t + 4\sqrt{t'^2 \cos^2\left(\frac{k_x a}{2}\right) + t'^2 \cos^2\left(\frac{k_y a}{2}\right)} \quad (4.9)$$

$$E_2 = V - t - 4\sqrt{t'^2 \cos^2\left(\frac{k_x a}{2}\right) + t'^2 \cos^2\left(\frac{k_y a}{2}\right)} \quad (4.10)$$

$$E_3 = V - t \quad (4.11)$$

When  $V_1 = V_3 \neq V_2$ , we call it the staggered case. For the staggered case with  $V_1 = V_3 = 0$  and  $V_2 = V$ , we get the eigenvalues as

$$E_1 = -t \quad (4.12)$$

$$E_2 = \frac{V - 2t + \sqrt{V^2 + 64t'^2(\cos^2\left(\frac{k_x a}{2}\right) + \cos^2\left(\frac{k_y a}{2}\right))}}{2} \quad (4.13)$$

$$E_3 = \frac{V - 2t - \sqrt{V^2 + 64t'^2(\cos^2\left(\frac{k_x a}{2}\right) + \cos^2\left(\frac{k_y a}{2}\right))}}{2} \quad (4.14)$$

If we consider the symmetric case where the the on-site energies at the three sites are equal, we can see that there is a point where the three bands touch. The three bands touch in a linear fashion i.e. the energy dispersion around that point is a linear function of the momentum. We put  $V_1 = V_2 = V_3 = 1$  and  $t = 1$ . The band touching point is  $(\pi, \pi)$ . Let us consider some momentum  $k = M + p$  where  $M$  is the band crossing point. Now, if we make a small momentum ( $|p| \ll 1$ ) expansion of the Hamiltonian around the band touching point, the low energy Hamiltonian upto first order of the expansion will be

$$H(k) \sim 2t' \begin{bmatrix} 0 & p_y & 0 \\ p_y & 0 & p_x \\ 0 & p_x & 0 \end{bmatrix} = 2t' L.B \quad (4.15)$$

where

$$L_x = \begin{bmatrix} 0 & 1 & 0 \\ 1 & 0 & 0 \\ 0 & 0 & 0 \end{bmatrix}, L_y = \begin{bmatrix} 0 & 0 & 0 \\ 0 & 0 & 1 \\ 0 & 1 & 0 \end{bmatrix}, L_z = \begin{bmatrix} 0 & 0 & i \\ 0 & 0 & 0 \\ -i & 0 & 0 \end{bmatrix} \quad (4.16)$$

$B = (p_x, p_y, 0)$  and  $L_x, L_y$  and  $L_z$  are pseudo spin-1 matrices which obey the SU(2) Lie algebra, which implies that the matrices satisfy the relation  $[L_i, L_j] = i\varepsilon_{ijk}L_k$ . This is similar to a Hamiltonian of a system having a spin  $L$  in an external magnetic field 'B'. If we calculate the eigenvalues of the low-energy Hamiltonian, we get the eigenvalues as  $\varepsilon = 0, \pm 2t' \sqrt{p_x^2 + p_y^2}$ . This can be re-written as  $\varepsilon = 2t'|p|m$  where  $m = 0, \pm 1$ . Thus, the energy eigenvalues of the low-energy Hamiltonian is quantized and mimicks that of a spin-1 system.

Now, if we consider the configuration with staggered potential, we can see that only two of the bands touch at a point. The flat band still exists but the band dispersion is not linear around the point. It is quadratic in character. Hence, such points are called quadratic band crossing point(QBCP). If we expand the low energy effective Hamiltonian around the point for the two bands can be witten as

$$H(k) \sim \frac{1}{m_0} \begin{bmatrix} p_x^2 & p_x p_y \\ p_x p_y & p_y^2 \end{bmatrix} = d_I I + d_x \sigma_x + d_z \sigma_z \quad (4.17)$$

where  $m_0 = \frac{(V_2 - t)}{4t'^2}$ ,  $\sigma$  are the Pauli matrices,  $I$  is the identity matrix.  $d_I = \frac{p_x^2 + p_y^2}{2m_0}$ ,  $d_x = \frac{p_x p_y}{m_0}$ ,  $d_z = \frac{p_x^2 - p_y^2}{2m_0}$  [14]. This Hamiltonian looks like a Dirac Hamiltonian. As we have been seen that there are band touching points in the dispersion. So, the next thing would be to understand the topological nature of the band touching points. The Berry phase for the band touching points can be calculated using

$$B^n = i \oint_C dp. \langle u_{np} | \nabla_p | u_{np} \rangle \quad (4.18)$$

around a contour C enclosing the band touching point in momentum space and  $|u_{np}\rangle$  denotes the Bloch eigenvector for the nth band where n is any of the bands involved in degeneracy. It can be shown that  $B^n = 2\pi$  for both of them[5].

QBCPs are the points of degeneracy in the bands. Let us define the Berry phase over a contour C

$$\exp\{(i\gamma_n(C))\} = \exp\left\{i \oint_C dR \langle n | \nabla | n \rangle\right\} \quad (4.19)$$

Now  $dS \nabla \times \langle n | \nabla | n \rangle$  looks like the flux linked. So, the area integral will give the charge enclosed. In our case, the term  $\nabla \times \langle n | \nabla | n \rangle$  can be identified as analogous to magnetic field. So, the the field will be because of a magnetic dipole.

Now points of degeneracy are the points of singularity in  $\nabla \times \langle n | \nabla | n \rangle$ . If we close a contour having a degeneracy, the Berry flux will be non-zero. The allowed values of Berry flux(=  $2W\pi$ ,  $W$  is the winding no. which is an integer) are quantized. Therefore, they cannot vary continuously when the contour is deformed adiabatically to a point. At a point, the Berry flux should be zero. So it has to be a constant or invariant. Therefore, contours having degeneracies cannot be shrunk to a point since there will be non-zero flux. Thus the points are topologically protected.

When  $B^n$  is non-zero, the band touching point is protected. It remains unaffected upon introducing weak perturbations.

The next logical step is to check if the QBCP survives when additional hoppings are allowed. We introduce diagonal hopping in the system

## 4.2 Effects of Additional Hopping

So, we introduce  $t''$  hopping in the system. When we have  $t''$  hopping in the model,i.e. from the dimer at site 1 in  $i$ th unit cell to the site 1 at  $(i+1)$ th unit cell or vice versa and same for the electrons at site 3, the additional part in the Hamiltonian is given by

$$H = -t'' \sum_i (c_{1bix}^\dagger c_{1a(i+1)x} + h.c) \quad (4.20)$$

where  $c_{1bix}^\dagger c_{1a(i+1)x}$  represents hopping from the site  $a$  in dimer at position 1 in the  $(i+1)$ th sublattice to the site  $b$  of dimer at position 1 in the  $i$ th sublattice along  $x$  direction. Using tight binding approximation for the  $t''$  hopping along  $y$  direction, we will get

$$H(k) = -t'' \sum_k (\cos(k_y a) a_{+k3}^\dagger a_{+k3} + i \sin(k_y a) a_{+k3}^\dagger a_{-k3} - i \sin(k_y a) a_{-k3}^\dagger a_{+k3} + \cos(k_y a) a_{-k3}^\dagger a_{-k3}) \quad (4.21)$$

Similarly along  $x$ -axis, we will get

$$H(k) = -t'' \sum_k (\cos(k_x a) a_{+k1}^\dagger a_{+k1} + i \sin(k_x a) a_{+k1}^\dagger a_{-k1} - i \sin(k_x a) a_{-k1}^\dagger a_{+k1} + \cos(k_x a) a_{-k1}^\dagger a_{-k1}) \quad (4.22)$$

Incorporating all these terms in the model, we get the new tight binding matrix as

$$\begin{pmatrix} V_1-t- & -4t' \cos(\frac{k_y a}{2}) & 0 & -it'' \sin(k_x a) & 0 & 0 \\ t'' \cos(k_x a) & V_2-t & -4t' \cos(\frac{k_x a}{2}) & 0 & 0 & 0 \\ -4t' \cos(\frac{k_y a}{2}) & V_2-t & -4t' \cos(\frac{k_x a}{2}) & 0 & 0 & 0 \\ 0 & -4t' \cos(\frac{k_x a}{2}) & V_3-t- & 0 & 0 & -it'' \sin(k_y a) \\ it'' \sin(k_x a) & 0 & t'' \cos(k_y a) & V_1+t+ & 0 & 0 \\ 0 & 0 & 0 & t'' \cos(k_x a) & 0 & 0 \\ 0 & 0 & 0 & 0 & V_2+t & 0 \\ 0 & 0 & it'' \sin(k_y a) & 0 & 0 & V_3+t+ \\ & & & & & t'' \cos(k_y a) \end{pmatrix} \quad (4.23)$$

We can see from the matrix that now  $a_-$  can hop from one site to another. This can be viewed as a process in which  $a_-$  changes into  $a_+$  and then the  $a_+$  electron hops. Also no extra symmetry is broken by introducing this hopping. The four fold symmetry is still there. Also one more important thing to note is that the terms  $a_+^\dagger a_-$  and  $a_-^\dagger a_+$  have opposite signs. The band structures have been plotted with parameters  $V_1 = V_3 = 0, V_2 = 1$  and  $t = t' = 1, t'' = 0.5$ .

### 4.2.1 Results

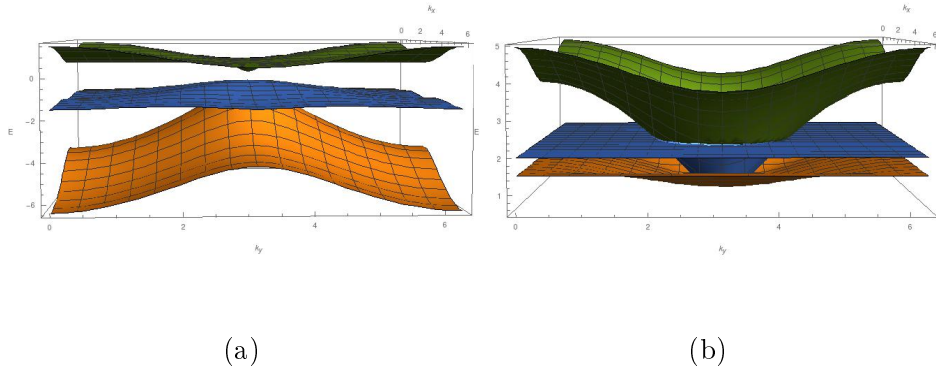


Figure 4.3: Dispersion relation for staggered case for a)  $a_+$  bands b)  $a_-$  bands with parameters ( $t = 1, t' = 1.0, t'' = 0.5, V_1 = V_3 = 0, V_2 = 1$ )

From the band structure, it is clear that the flat band acquires a dispersion which was previously dispersionless. However, the quadratic band crossing point(QBCP) still remains unaffected. However, new topologically important features come up in the band structure. Tilted Dirac cones can be seen in the band dispersion which is evident from the cross section of the band

dispersions (4.4). The QBCP is at a point  $(\pi, \pi)$  which lies at the boundary of the first Brillouin zone.

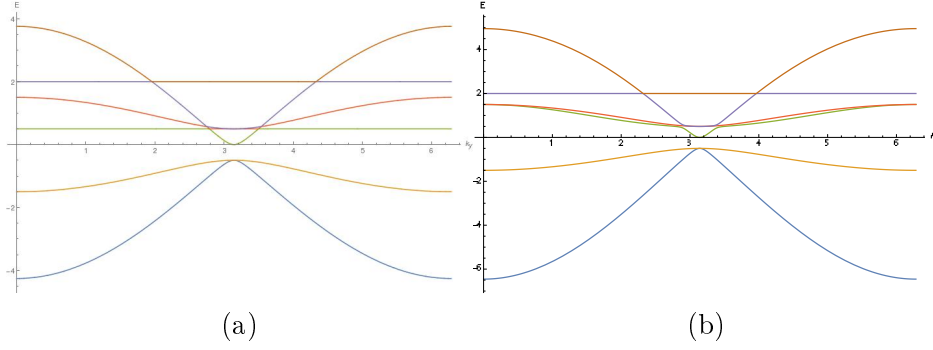


Figure 4.4: Cross section of the band structure through the a) plane  $k_x = \pi$  and b) the diagonal plane ( $k_x = k_y$ ) with parameters  $t = 1, t' = 1.0, t'' = 0.5, V_1 = V_3 = 0, V_2 = 1$ . The band crossing point of the two lower  $a_+$  bands at  $(\pi, \pi)$  is a QBCP. Two  $a_-$  bands touch at a surface.

The top three bands in the cross section are  $a_-$  and the lowest three ones are  $a_+$ . There is band inversion which can be seen. There are three band inversions which is evident from the cross sectional view(4.4). Number of band inversions are important if one wants to calculate the topological  $Z_2$  index. The Fermi surfaces have been plotted for  $\omega$  corresponding to the Von-Hove singularities in the density of states. The Fermi surfaces show interesting features.

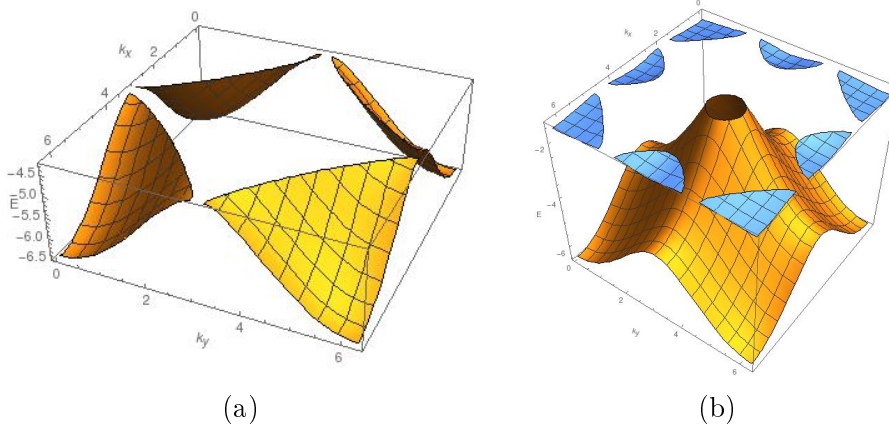


Figure 4.5: Fermi surface for the  $a_+$  bands for Von-Hove singularity at a)  $\omega = -4.275$  and at b)  $\omega = -1.3659$  for parameters  $t = 1, t' = 1.0, t'' = 0.5, V_1 = V_3 = 0, V_2 = 1$

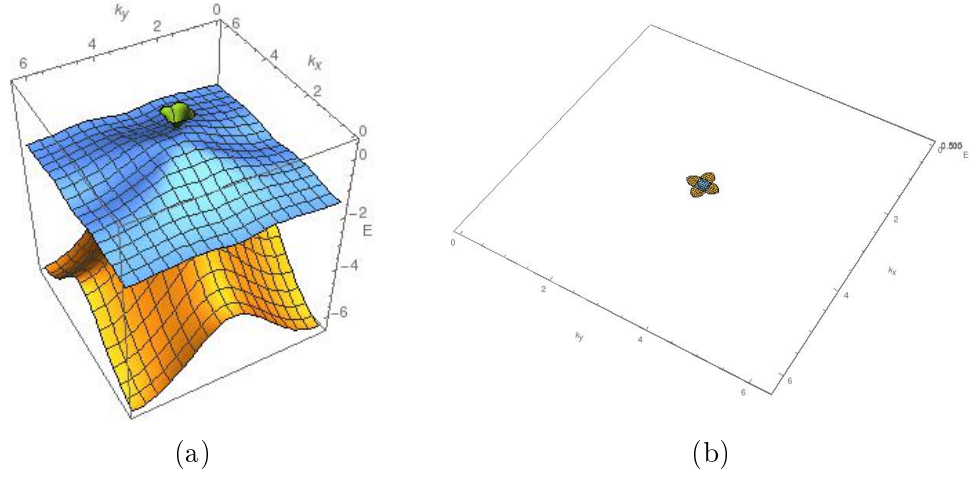


Figure 4.6: Fermi surface for the  $a_+$  bands for Von-Hove singularity at a)  $\omega = 0.488$  and for the  $a_-$  bands at b)  $\omega = 0.5$  for parameters  $t = 1, t' = 1.0, t'' = 0.5, V_1 = V_3 = 0, V_2 = 1$

For the  $a_-$  bands in the figure above, there are two elliptical pockets which are perpendicular to each other. On top of this, there is a circular pocket. The Fermi surfaces will help us predict various properties. Existence of such kind of Fermi surfaces will help us map various properties of the dimer model in the real system. This kind of Fermi surfaces have been seen in Bi-square net [15]. Also similar to the Bi-net structure, the band structure has anisotropic Dirac cones.

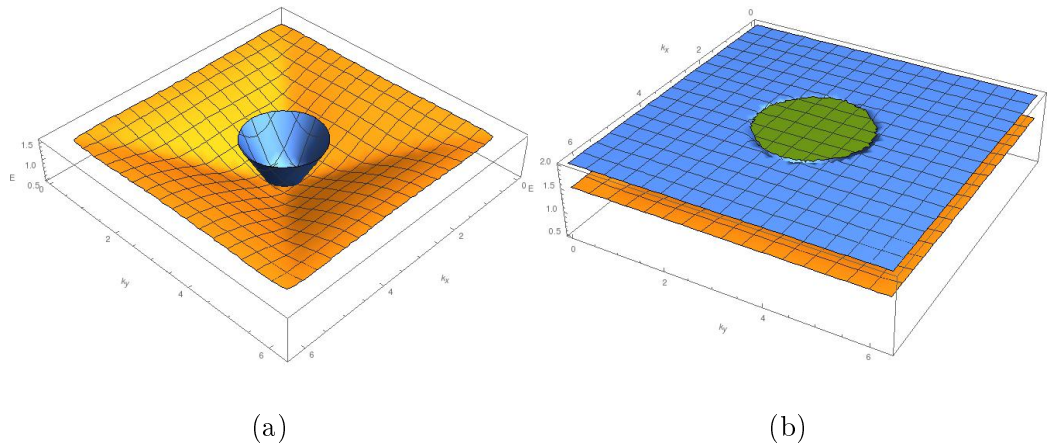


Figure 4.7: Fermi surface for  $a_-$  bands with  $(t = 1, t' = 1.0, t'' = 0.5, V_1 = V_3 = 0, V_2 = 1)$  for Von-Hove singularity at a)  $\omega = 1.4809$  and b)  $\omega = 2$

The top surface for the Fermi surface at  $\omega = 2$  looks like a flat surface. Therefore, it corresponds to the delta peak in the density of states. The edges are also dispersionless.

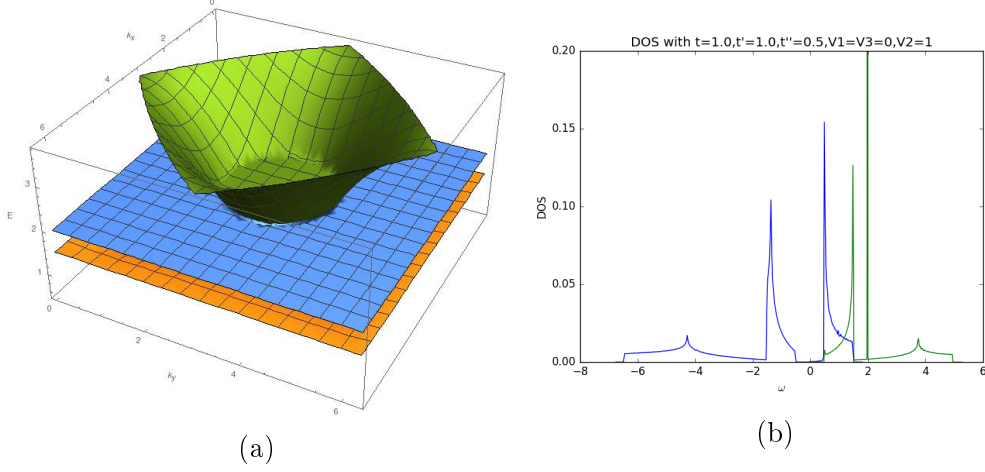


Figure 4.8: a) Fermi surface for  $a_-$  with  $(t = 1, t' = 1.0, t'' = 0.5, V_1 = V_3 = 0, V_2 = 1)$  for Von-Hove singularity at  $\omega = 1.4809$  and b) DOS for all the bands.

The blue part in the DOS plot corresponds to the  $a_+$  bands and the green one for the  $a_-$ . Here we plot the band structure for  $t = 1, t' = 0.75, t'' = -0.5, V_1 = V_2 = V_3 = 1$  (symmetric configuration). In this case, only the lower two  $a_+$  bands touch at a QBCP. In the  $a_-$  bands, we can see tilted Dirac cones.

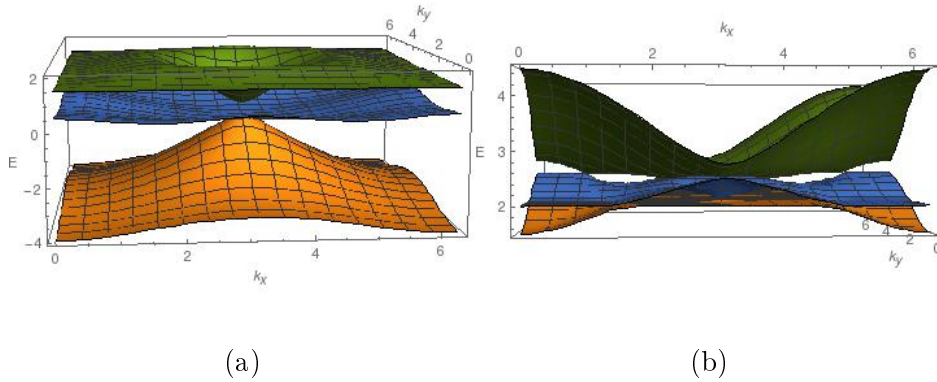


Figure 4.9: Dispersion relation for symmetric case for (a)  $a_+$  bands and (b)  $a_-$  bands with parameters  $V_1 = V_2 = V_3 = 1, t = 1, t' = 0.75, t'' = -0.5$

Among the  $a_+$  bands, only lower two bands touch at point. The touching point is a QBCP. Because of  $t''$  hopping, the flat band acquires dispersion. Along the  $k_x = \pi$  plane, there are anisotropic Dirac cones. However, one interesting thing to observe is that there is a surface touching between the top  $a_-$  bands.

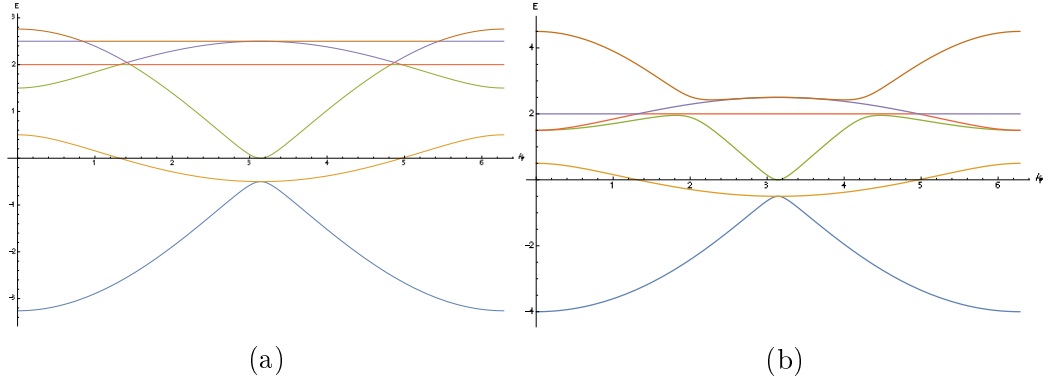


Figure 4.10: Cross section of the band structure for through a) plane  $k_x = \pi$  and b) plane  $k_x = k_y$  with parameters  $V_1 = V_2 = V_3 = 1, t = 1, t' = 0.75, t'' = -0.5$

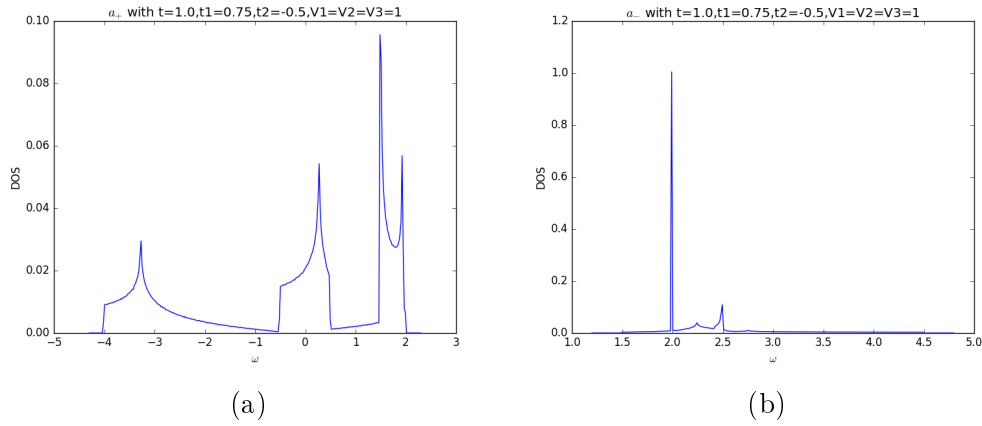


Figure 4.11: DOS for a)  $a_+$  and b)  $a_-$  bands with parameters  $V_1 = V_2 = V_3 = 1, t = 1, t' = 0.75, t'' = -0.5$

The lower part of the DOS resembles that of a two-dimensional band. There are four Von-Hove singularities in the density of states for  $a_+$  bands and four for  $a_-$  bands. There are electron pockets which can be seen in the Fermi surface plots.



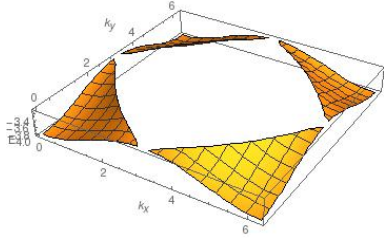


Figure 4.12: Fermi surface for symmetric case for lower bands with  $(t = 1, t' = 0.75, t'' = -0.5)$  for Von-Hove singularity at  $\omega = -3.266$

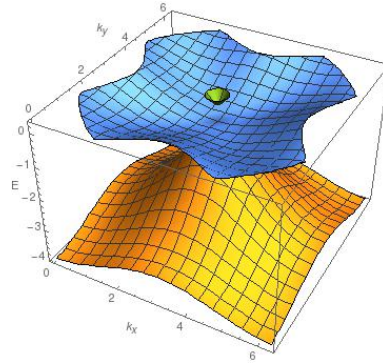


Figure 4.13: Fermi surface for symmetric case for lower bands with  $(t = 1, t' = 0.75, t'' = -0.5)$  for Von-Hove singularity at  $\omega = 0.276$

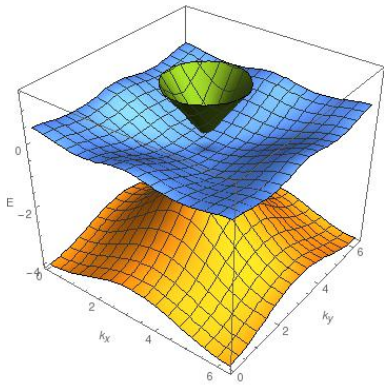


Figure 4.14: Fermi surface for symmetric case for lower bands with  $(t = 1, t' = 0.75, t'' = -0.5)$  for Von-Hove singularity at  $\omega = 1.486$

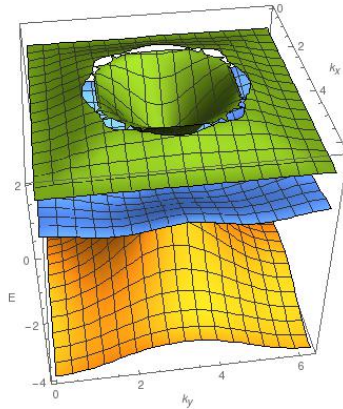


Figure 4.15: Fermi surface for symmetric case for lower bands with  $(t = 1, t' = 0.75, t'' = -0.5)$  for Von-Hove singularity at  $\omega = 1.926$

Now if we consider the Fermi surface at  $\omega = 2.244$ , it can be seen that there is Fermi surface nesting. This is because the blue bands (in the corners) in the figure disperses only along one direction. So using a nesting vector, it can be taken the other end.

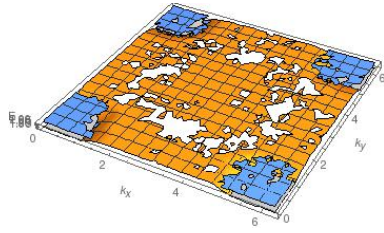


Figure 4.16: Fermi surface for symmetric case for top bands with  $(t = 1, t' = 0.75, t'' = -0.5)$  for Von-Hove singularity at  $\omega = 1.992$

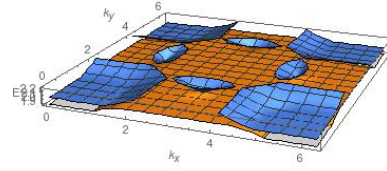


Figure 4.17: Fermi surface for symmetric case for top bands with  $(t = 1, t' = 0.75, t'' = -0.5)$  for Von-Hove singularity at  $\omega = 2.244$

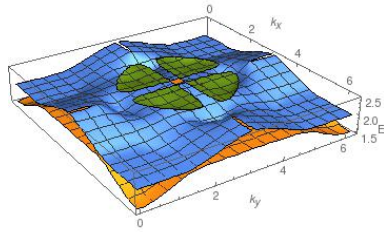


Figure 4.18: Fermi surface for symmetric case for top bands with  $(t = 1, t' = 0.75, t'' = -0.5)$  for Von-Hove singularity at  $\omega = 2.496$

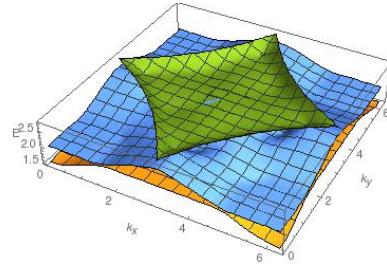


Figure 4.19: Fermi surface for symmetric case for top bands with  $a(t = 1, t' = 0.75, t'' = -0.5)$  for Von-Hove singularity at  $\omega = 2.76$

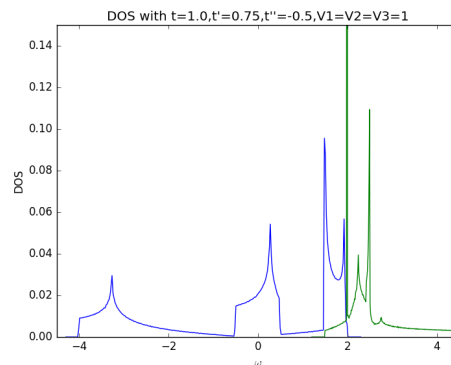


Figure 4.20: DOS(zoomed view) for symmetric case with  $t = 1, t' = 0.75, t'' = -0.5$

The next case is when the intra-dimer hopping is equal to the nearest inter-dimer hopping. The parameters are  $V_1 = V_2 = V_3 = 1, t = t' = 1.0, t'' = -0.5$ .

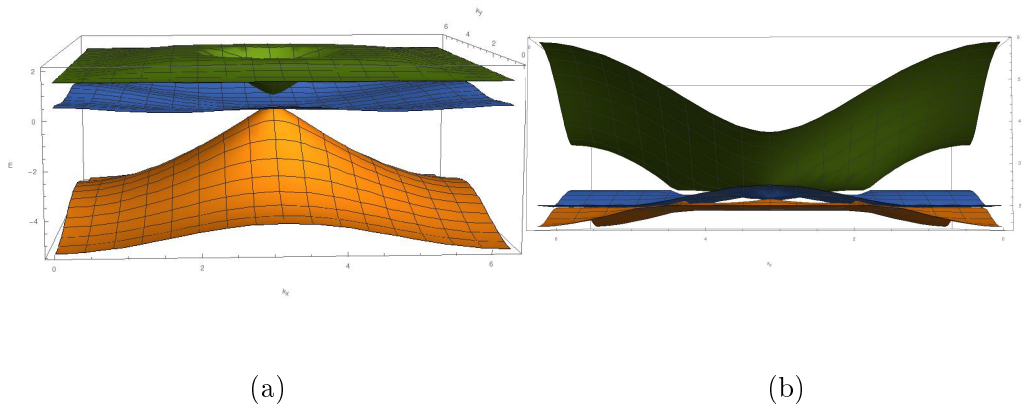


Figure 4.21: Band structure for a)  $a_+$  and b)  $a_-$  bands with parameters  $V_1 = V_2 = V_3 = 1, t = 1, t' = 1, t'' = -0.5$

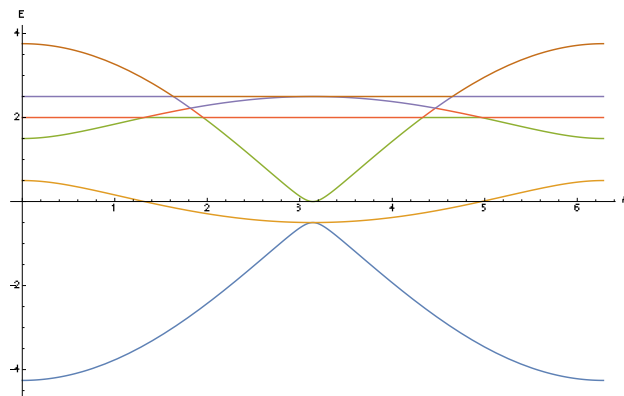


Figure 4.22: Cross section of the band dispersions for through the plane  $k_x = \pi$  with  $(t = 1, t' = 1.0, t'' = -0.5)$

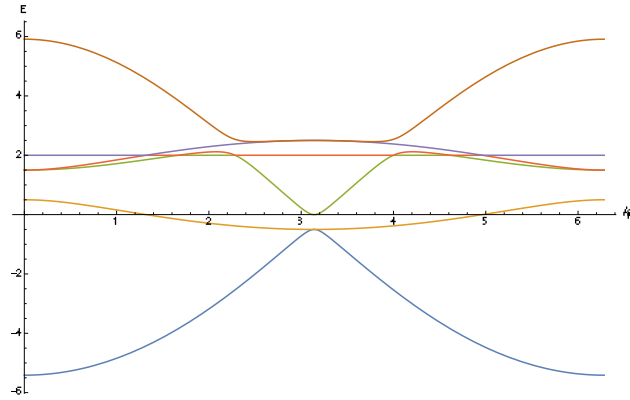


Figure 4.23: Cross section of the band dispersions for through the diagonal plane  $k_x = k_y$  with  $(t = 1, t' = 1.0, t'' = -0.5)$

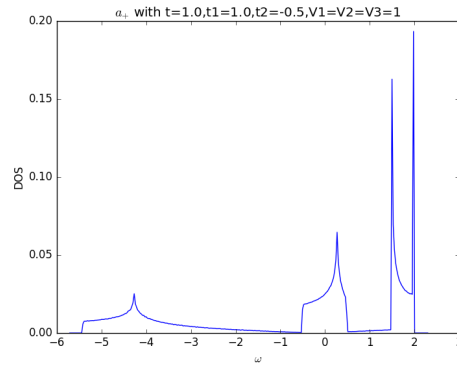


Figure 4.24: DOS for symmetric case for  $a_+$  bands  $(t = 1, t' = 1.0, t'' = -0.5)$

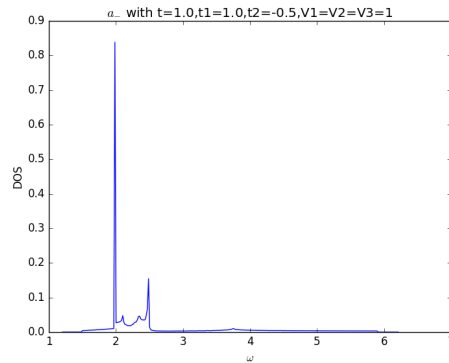


Figure 4.25: DOS for symmetric case for  $a_-$   $(t = 1, t' = 1.0, t'' = -0.5)$

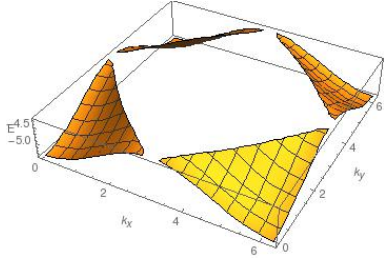


Figure 4.26: Fermi surface for symmetric case for  $a_+$  bands ( $t = 1, t' = 1.0, t'' = -0.5$ ) for Von-Hove singularity at  $\omega = -4.27$

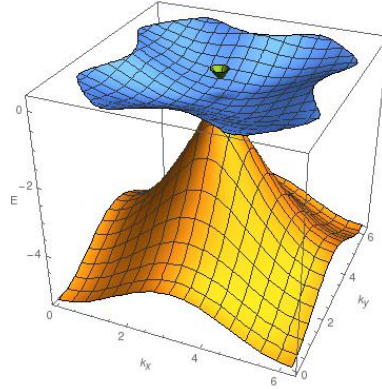


Figure 4.27: Fermi surface for symmetric case for  $a_-$  bands with ( $t = 1, t' = 1.0, t'' = -0.5$ ) for Von-Hove singularity at  $\omega = 0.27$

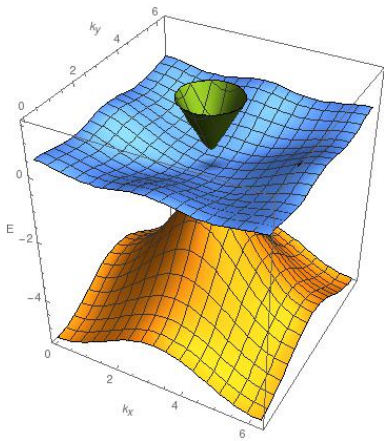


Figure 4.28: Fermi surface for symmetric case for  $a_+$  bands ( $t = 1, t' = 1.0, t'' = -0.5$ ) for Von-Hove singularity at  $\omega = 1.5$

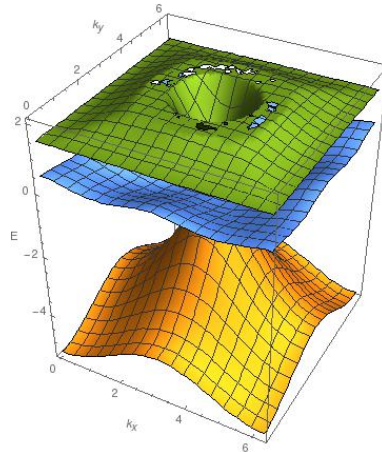


Figure 4.29: Fermi surface for symmetric case for  $a_+$  bands ( $t = 1, t' = 1.0, t'' = -0.5$ ) for Von-Hove singularity at  $\omega = 2$

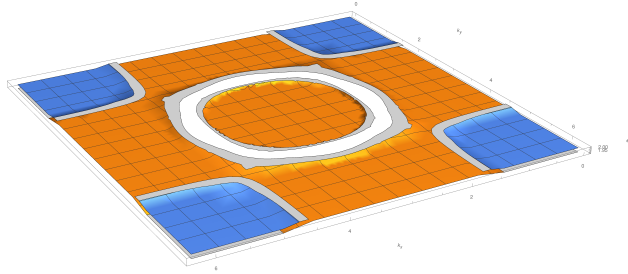


Figure 4.30: Fermi surface for symmetric case for  $a_-$  band with  $t = 1, t' = 1.0, t'' = -0.5$  for Von-Hove singularity at  $\omega = 2.1$

This is one of the most interesting Fermi surfaces. The Fermi surface has three pockets. The outer one is open. There are two inner pockets. This type of Fermi surface is found in Strontium Ruthenate. Recently, calculations have been done to get the Fermi surface [16]. The Fermi surface is because of the  $a_-$  which is odd under inversion.

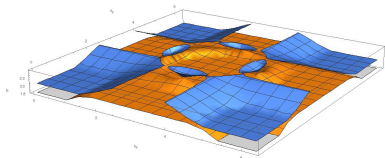


Figure 4.31: Fermi surface for symmetric case for  $a_-$  band with  $t = 1, t' = 1.0, t'' = -0.5$  for Von-Hove singularity at  $\omega = 2.35$

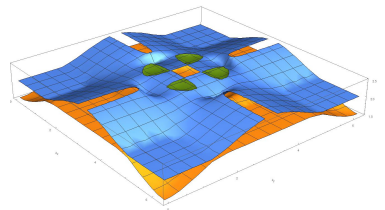


Figure 4.32: Fermi surface for symmetric case for  $a_-$  bands with  $t=1, t'=1.0, t''=-0.5$  for Von-Hove singularity at  $\omega = 2.4865$

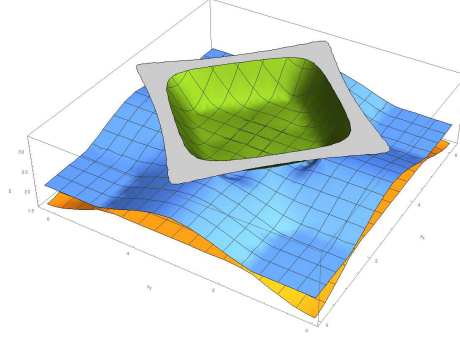


Figure 4.33: Fermi surface for symmetric case for  $a_-$  bands with  $(t = 1, t' = 1.0, t'' = -0.5)$  for Von-Hove singularity at  $\omega = 3.75$

## 4.2.2 Diagonal hopping

If we have a diagonal hopping instead of an hopping to the opposite side, we get some interesting features in the band structure.

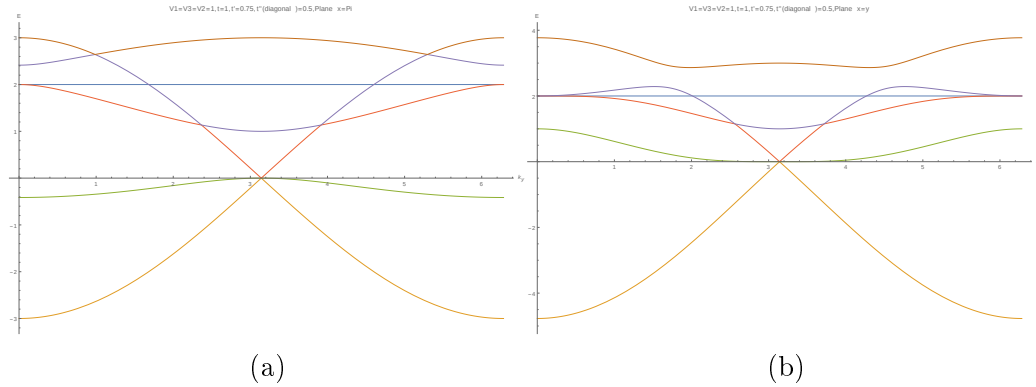


Figure 4.34: Cross section of the band dispersions for through the diagonal plane a)  $k_x = \pi$  and b)  $k_x = k_y$  with  $V_1 = V_2 = V_3 = 1, t = 1, t' = 0.75, t'' = 0.5$ ,  $t''$  is the diagonal hopping parameter

In the band structure, we can see that three bands touch at a single band. However, the middle band acquires dispersion and have a quadratic behaviour around the band touching point. This kind of band structure has been found in  $K_4$  lattice[17]. So, this kind of band touching points can be realized in this model. Also many anisotropic Dirac cones come up. By anisotropic, I mean the curvature of the cones are different in different directions. One thing to note is that the Hamiltonian has four fold symmetry. So there will be four such points instead of two as seen in the cross sectional cuts.

### 4.3 Effects of Electric Field

In order to check the stability of the the QBCPs or other topologically important points, we introduce the effect of an electric field. The electric field  $E_z$  is turned on in a direction perpendicular to the plane of the Lieb lattice. Now the effect of electric effect will to polarize. Consider the displacements of site a and site b in the dimer as  $X_a$  and  $X_b$  respectively.

$$H = \sum_{j=1,2,3}^i g(X_a n_{jai} + X_b n_{jbi}) \quad (4.24)$$

where  $n_{jai} = c_{jai}^\dagger c_{jai}$  is the number operator for the site a of the dimer at position j in the  $i$ th unit cell and  $g$  is nothing but the interaction strength. If we make a transformation about the centre of mass such that  $\frac{X_a + X_b}{2} = X_+$  and  $\frac{X_a - X_b}{2} = X_-$  and use  $a_+, a_-$ , we will get the Hamiltonian in momentum space as

$$H = \sum_{j=1,2,3}^k gX_+(n_{+jik} + n_{-jk}) + gX_-(a_{+jk}^\dagger a_{-jk} + a_{-jk}^\dagger a_{+jk}) \quad (4.25)$$

where  $n_{+ji} = a_{+ji}^\dagger a_{+ji}$ . The Hamiltonian is no longer invariant under inversion. This is because of the mixing term. Both  $a_{+k}^\dagger a_{-k}$  and its hermitian conjugate has the same sign. So inverting them doesn't keep the Hamiltonian same. By inverting, it means that site a goes to site b and site b goes to site a with respect to the centre of mass. The new tight binding matrix in momentum space will be given by:

$$\begin{pmatrix} V_1 - t + gX_{+-} & -4t' \cos(\frac{k_y a}{2}) & 0 & -it'' \frac{\sin(k_x a)}{gX_-} & 0 & 0 \\ t'' \cos(k_x a) & V_2 - t + gX_+ & -4t' \cos(\frac{k_x a}{2}) & 0 & gX_- & 0 \\ -4t' \cos(\frac{k_y a}{2}) & V_3 - t + gX_{+-} & t'' \cos(k_y a) & 0 & 0 & -it'' \frac{\sin(k_y a)}{gX_-} \\ 0 & -4t' \cos(\frac{k_x a}{2}) & 0 & 0 & 0 & 0 \\ it'' \frac{\sin(k_x a)}{gX_-} & 0 & 0 & V_1 + t + gX_{++} & 0 & 0 \\ 0 & gX_- & 0 & t'' \cos(k_x a) & 0 & 0 \\ 0 & 0 & it'' \frac{\sin(k_y a)}{gX_-} & 0 & V_2 + t + gX_+ & 0 \\ 0 & 0 & 0 & 0 & 0 & V_3 + t + gX_{++} \\ & & & & & t'' \cos(k_y a) \end{pmatrix} \quad (4.26)$$



### 4.3.1 Results

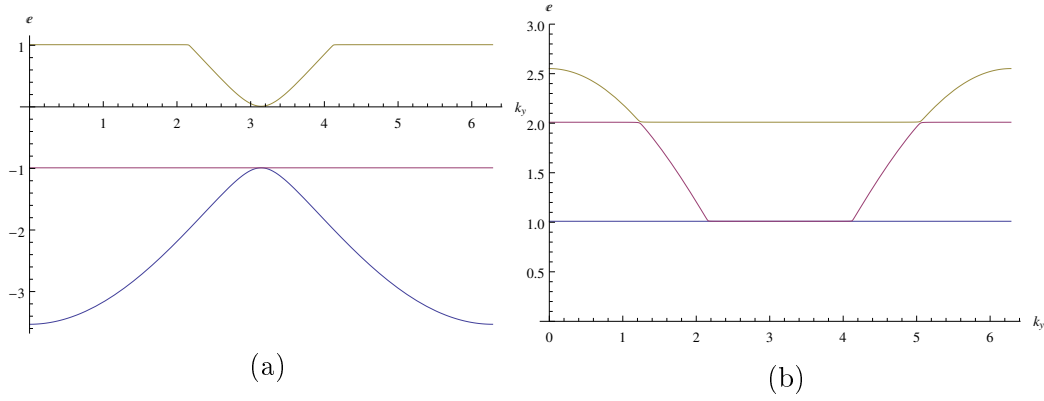


Figure 4.35: a) Cross section for the (a)  $a_+$  bands and (b)  $a_-$  bands in the band structure with parameters  $t = 1, t' = 0.75, t'' = 0, g = 0.2, V_1 = V_3 = 0, V_2 = 1$

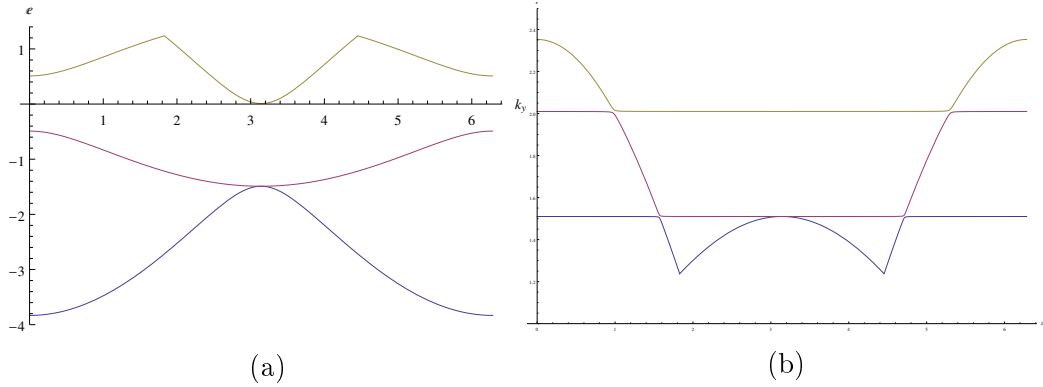


Figure 4.36: a) Cross section for the (a)  $a_+$  bands and (b)  $a_-$  bands in the band structure with parameters  $t = 1, t' = 0.75, t'' = -0.5, g = 0.2, V_1 = V_3 = 0, V_2 = 1$

It can be seen that the dirac cones become gapped once the electric field is introduced. This is because of the hybridisation. The hybridisation goes as  $\sin(k)$  which is an odd function. Thus at time reversal invariant momenta, it goes to zero and the gap closes. When there is electric field, the inversion symmetry is broken and then the gap becomes non-zero at special points. Now it can be seen that when the electric field is high, the gaps are more prominent. However, the QBCP still stays the same. It is stable under the action of electric field.

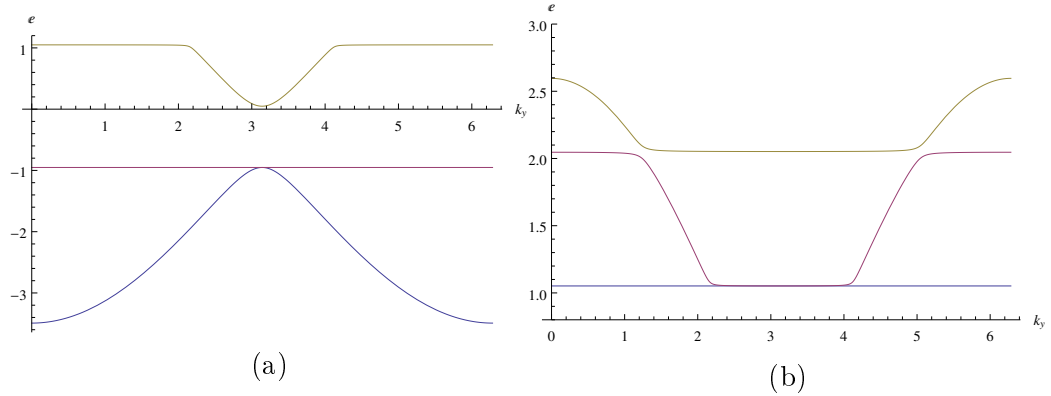


Figure 4.37: a) Cross section for the (a)  $a_+$  bands and (b)  $a_-$  bands in the band structure with parameters  $t = 1, t' = 0.75, t'' = 0, g = 1, V_1 = V_3 = 0, V_2 = 1$

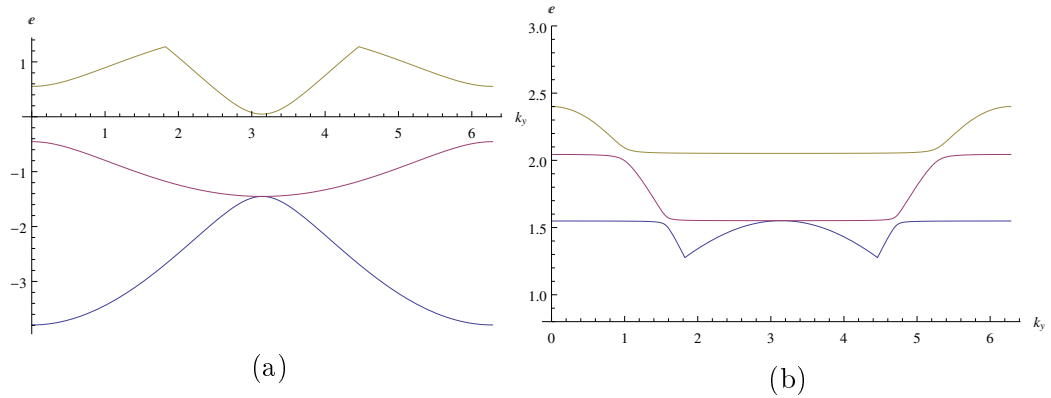


Figure 4.38: a) Cross section for the (a)  $a_+$  bands and (b)  $a_-$  bands in the band structure with parameters  $t = 1, t' = 0.75, t'' = -0.5, g = 1, V_1 = V_3 = 0, V_2 = 1$

## 4.4 Rashba term

Rashba effect is generally defined as the phenomenon of momentum dependent splitting of bands. The Rashba term arises because of breaking of centrosymmetry. If we think  $a_1$  as creation operator of spin up fermions.  $(a_{+1}^\dagger a_{+2})$  will act as a spin flip operator where an  $a_1$  is flipped to  $a_2$ . Using this analogy, we can conclude that  $a_{+1}^\dagger a_{+2} + h.c$  will act as  $\sigma_x$  where  $\sigma_x$  is the x-component of an orbital pseudospin. Similarly,  $i(a_{+1}^\dagger a_{+2} - h.c)$  will act as the y component of the pseudospin. And in the low momentum region,

$\sin(k) \sim k$ . Hence, the Hamiltonian can be written as

$$H_r = -eEa \sum_k [\sin(k_y/2)(a_{+k1}^\dagger a_{+k2} + h.c.) - i \sin(k_x/2)(a_{+k1}^\dagger a_{+k2} - h.c.)] \quad (4.27)$$

Here 1 and 2 in the subscript labels the bands involved in degeneracy of the + bands at a point. Rashba term in the Hamiltonian will be introduced in the Hamiltonian between the bands involved in the band touching point. If we remember the QBCP in the simplest case, only the lower two  $a_+$  bands touch. In order to investigate the effects of this term, we start with the simplest case with no other hopping. We are considering a Lieb lattice (with no dimers). The first case involves only two hoppings  $t$  and  $t'$  where  $t$  is the nearest neighbour hopping and  $t'$  is the diagonal hopping between sites 1 and 3 in the Lieb lattice.

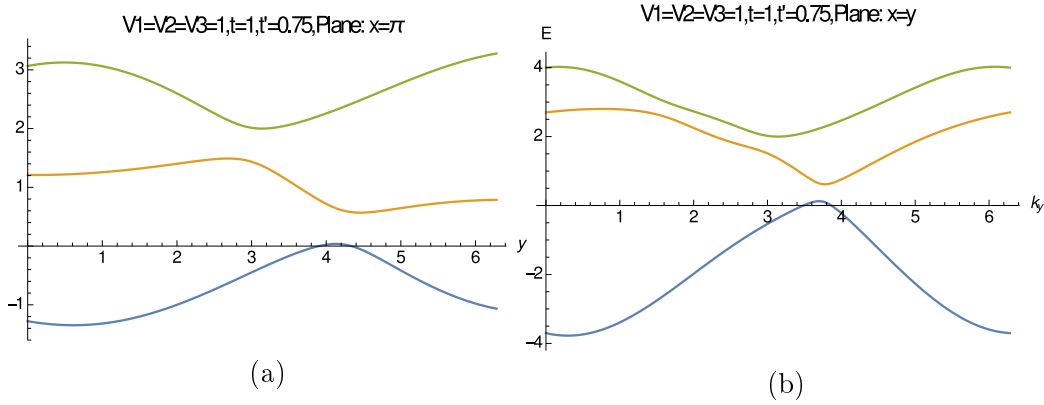


Figure 4.39: a) Cross section of the bands with  $(V_1 = V_2 = V_3 = 1, t = 1, t' = 0.75, m = 0.5, g = 0.5)$  through plane  $k_x = \pi$  and b) diagonal plane  $k_x = k_y$

For the results obtained above and below for both the symmetric and staggered case, the strength of the electric field, denoted by  $g$ , and the strength of Rashba coupling, denoted by  $m$ , are both equal to 0.5. The results here are for a Lieb lattice without the dimers.

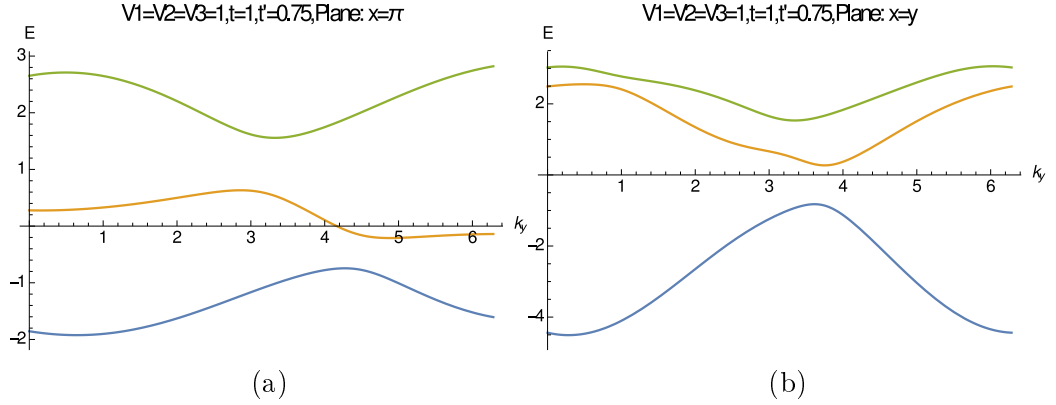


Figure 4.40: a) Cross section of the bands with  $(V_1 = V_3 = 0, V_2 = 1, t = 1, t' = 0.75, m = 0.5, g = 0.5)$  through plane  $k_x = \pi$  and b) diagonal plane  $k_x = k_y$

We can see that because of the Rashba term, both the Dirac point and QBCP becomes gapped. Since, this is valid for the simplest case, the same argument can be used for the dimer case. We now introduce the Rashba term in the dimer model on Lieb lattice. We consider the case with only one intra-dimer hopping and two nearest neighbour inter-dimer hopping one of which is the diagonal hopping.

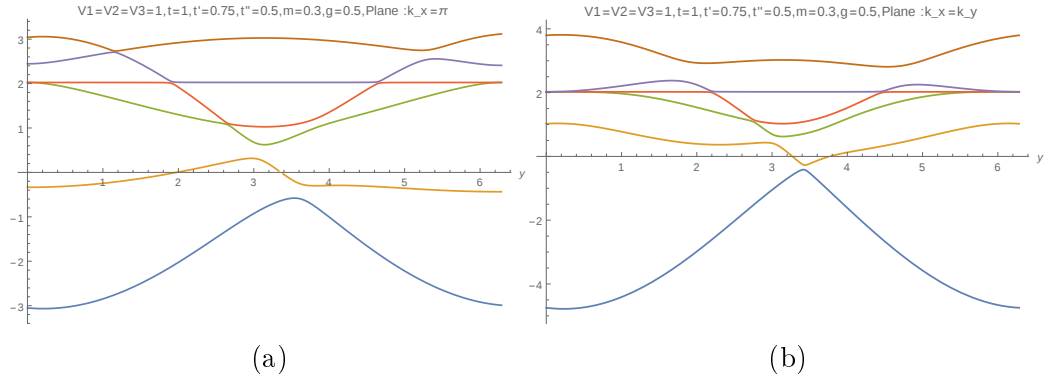


Figure 4.41: a) Cross section of the bands with  $(V_1 = V_2 = V_3 = 1, t = 1, t' = 0.75, t'' = 0.5, m = 0.3, g = 0.5)$  through plane  $k_x = \pi$  and b) diagonal plane  $k_x = k_y$ . Here  $t''$  is the diagonal hopping.

We know from the diagonal hopping case, that there was a triple band touching point at  $(\pi, \pi)$ . This point becomes gapped upon introduction of Rashba coupling in presence of electric field. The Dirac points become gapped. However, one interesting fact to notice is that the band touching

point at  $(\pi, 0)$  and tripple band touching point at  $(0, 0)$  and  $(2\pi, 2\pi)$  retain their character. The QBCP at  $(\pi, 0)$  maintains its spin- $\frac{1}{2}$  structure despite the symmetry breaking terms. Similarly, the tripple band crossing point has a spin-1 structure which remains preserved.

## 4.5 Haldane Model

Quantum Hall effect is usually seen in two dimensional electron systems when there is a uniform external magnetic field. However, Haldane showed that the same can be obtained without any magnetic flux through the unit cell by breaking time reversal symmetry.

Consider a honeycomb-net model which can be seen in 2D graphite. It consists of two sub-lattices A and B. Let the nearest neighbor hopping parameter be  $t_1$  and the next nearest hopping parameter be  $t_2$ . The on-site energy on sites A and B be  $V+M$  and  $V-M$  respectively, where  $V$  is the average potential and  $M$  is the inversion symmetry breaking on-site energy. So, without loss of generality,  $V$  can be set to 0. In order to break the time-reversal symmetry, a magnetic flux density  $B$  is introduced perpendicular to the plane of graphite. The magnetic flux through the unit cell is zero. This is one of the assumption.

When a particle moves around a closed contour enclosing a flux, it acquires a phase  $\exp\{i(e/\hbar \int A.dr)\}$ [18], where  $A$  is the vector potential. A next nearest complex hopping is introduced. So, in this case, the flux enclosed by the  $t_2$  hopping will have a non-zero phase. Consider the displacements  $a_1, a_2, a_3$  from site B to nearest site A. Define  $b_1 = a_2 - a_3, b_2 = a_3 - a_1$ , where  $b_i$ s are the next nearest displacements. If we consider all of these, the Hamiltonian[19] can be written as

$$H(k) = 2t_2 \cos \phi \left[ \sum_i \cos(k.b_i) \right] I + t_1 \left[ \sum_i [\cos(k.a_i) \sigma_x + \sin(k.a_i) \sigma_y] \right] + [M - 2t_2 \sin \phi \sum_i \sin(k.b_i)] \sigma_z \quad (4.28)$$

The two bands will touch at degenerate points if all the coefficients of the  $\sigma$  become zero at the zone boundaries. Using this, one can find that the this happens when  $|M| = |3\sqrt{3}t_2 \sin \phi|$ . This marks a topological transition in the system. Now we will apply the same logic in our dimer model on Lieb lattice.

We consider the spin half case. Initially, the low energy Hamiltonian for the staggered case near the QBCP could be written as

$$H_0 = d_0\sigma_0 + d_x\sigma_x + d_z\sigma_z \quad (4.29)$$

where  $\sigma_0$  is the identity operator. When there is Rashba spin orbit coupling, we get terms in the Hamiltonian like

$$-e\epsilon a \sum_k \left[ \sin\left(\frac{k_y}{2}\right) (a_{k1}^\dagger a_{k2} + a_{k2}^\dagger a_{k1}) - i \sin\left(\frac{k_x}{2}\right) (a_{k1}^\dagger a_{k2} - a_{k2}^\dagger a_{k1}) \right] \quad (4.30)$$

The term  $(a_{k1}^\dagger a_{k2} + a_{k2}^\dagger a_{k1})$  can be identified as  $\sigma_x$  for a pseudospin. Similarly,  $-i(a_{k1}^\dagger a_{k2} - a_{k2}^\dagger a_{k1}) \rightarrow \sigma_y$ . After incorporating the Rashba spin-orbit coupling term in the Hamiltonian

$$H_0 = d_0\sigma_0 + [d_x(k) - e\epsilon a \sin\left(\frac{k_y}{2}\right)] \cdot \sigma_x + e\epsilon a \sin\left(\frac{k_x}{2}\right) \cdot \sigma_y + d_z\sigma_z \quad (4.31)$$

Since the Hamiltonian under consideration is for small momentum,  $\sin(k) \sim k$ . If the y-component of the pseudospin is kept fixed and the x and z axis rotated by  $\frac{\pi}{2}$ , then  $\sigma_x \rightarrow \sigma_z$  and  $\sigma_z \rightarrow -\sigma_x$ . The new Hamiltonian will be

$$H = d_0(k)\sigma_0 - d_z(k)\sigma_x + e\epsilon a k_x \sigma_y + [d_x(k) - e\epsilon a k_y] \sigma_z \quad (4.32)$$

We know that the coefficient of  $\sigma_z$  gives us the mass term.

As  $\epsilon$  increases, there will be a point where the mass term will change sign which will mark the topological transition.

# Chapter 5

## Extensions of the model

### 5.1 Two-orbital model

As we have been seen in the previous case, upon the transformation, there were two kinds of electron. One belonging to the  $a_+$  band and other to the  $a_-$ . So, if we remember  $a_+ = \frac{c_a + c_b}{\sqrt{2}}$ . Now if we invert the dimer with respect to its center of mass i.e.  $a \rightarrow b$  and  $b \rightarrow a$ ,  $a_+$  remains the same. However,  $a_-$  picks up a negative sign. So, it is evident that  $a_+$  is even under inversion whereas  $a_-$  is odd.

Now the next thing would be to map the previous model with dimers to a model having two orbitals at each site. Let us name them as  $a$  and  $b$ . One of the orbitals, "a", is even under parity and the other odd. We will first begin with the simplest case i.e. only nearest neighbour hopping and then will consider other hopping. For consistency with the dimer model, we demand that only electrons in  $a$  orbital hop. So, the Hamiltonian can be written as

$$H_{kin} = -t \sum_i (c_{ai1y}^\dagger c_{ai2y} + c_{ai2x}^\dagger c_{ai3x} + c_{ai1y}^\dagger c_{a(i+1)2y} + c_{a(i+1)3x}^\dagger c_{ai2x}) + h.c. \quad (5.1)$$

$$H_{total} = H_{kin} + \sum_i V_1 c_{ai1}^\dagger c_{ai1} + V_2 c_{ai2}^\dagger c_{ai2} + V_3 c_{ai2}^\dagger c_{ai2} \quad (5.2)$$

The tight binding Hamiltonian in matrix form for the lattice in momentum space is

$$H(k) = \begin{bmatrix} V_1 & -2t' \cos\left(\frac{k_y}{2}\right) & 0 \\ -2t' \cos\left(\frac{k_y}{2}\right) & V_2 & -2t' \cos\left(\frac{k_x}{2}\right) \\ 0 & -2t' \cos\left(\frac{k_x}{2}\right) & V_3 \end{bmatrix} \quad (5.3)$$

Let us first consider the staggered case i.e.  $V_1 = V_3 = V$ . The eigenvalues of the matrix are  $E = V, E_+ = \frac{(V_2-V)+\sqrt{(V_2-V)^2-4V_2V+16t'^2(\cos^2(\frac{k_x}{2})+\cos^2(\frac{k_y}{2}))}}{2}, E_- = \frac{(V_2-V)-\sqrt{(V_2-V)^2-4V_2V+16t'^2(\cos^2(\frac{k_x}{2})+\cos^2(\frac{k_y}{2}))}}{2}$

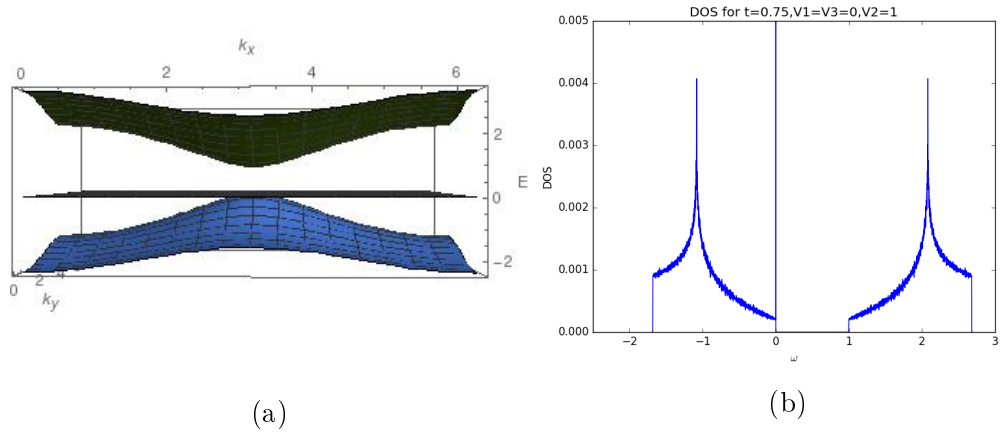


Figure 5.1: a) Band dispersion of the ‘a’ bands in region  $[0, 2\pi]$  for staggered case and (b) density of states with  $t = 1, V_1 = V_3 = 0, V_2 = 1$

The band structure shows a quadratic band crossing point(QBCP). The QBCP is at  $(\pi, \pi)$ . There is a flat band, which is dispersionless. The density of states have also been plotted for the bands. The edges of the density of states resemble that of a two dimensional band. The two dimensional character is evident from the band dispersion dispersion plot. The band disperses along both  $k_x$  and  $k_y$ . The delta function in the density of states corespond to the flat band. At the band touching point, the density of states is non-zero. This has important implications when the interaction effects are considered. We would like to investigate the Fermi surface at the Von-Hove singularities. There are two Von-Hove singularities in this case. The fermi surfaces corresponding to the two Von-Hove singularities have been plotted. There are pockets.



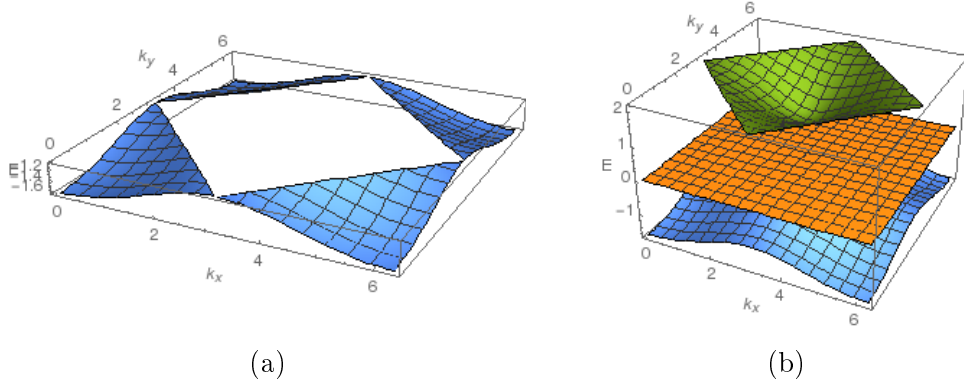


Figure 5.2: Fermi surface for Von-Hove singularity a)at  $\omega = -1.08$  and b) $\omega = 2.0808$  with ( $t = 0.75, V1 = V3 = 0, V2 = 1$ )

If we put  $V = 0$ , we get the orthonormalised eigenvector corresponding to  $E = V$  (flat band),  $E_+$  and  $E_-$  respectively are

$$\begin{bmatrix} \frac{\cos(\frac{k_x}{2})}{\sqrt{\cos^2(\frac{k_x}{2}) + \cos^2(\frac{k_y}{2})}} \\ 0 \\ \frac{\cos(\frac{k_y}{2})}{\sqrt{\cos^2(\frac{k_x}{2}) + \cos^2(\frac{k_y}{2})}} \end{bmatrix}, \begin{bmatrix} \frac{\cos(\frac{k_y}{2})}{\sqrt{\cos^2(\frac{k_x}{2}) + \cos^2(\frac{k_y}{2}) + E_+^2}} \\ \frac{\cos(\frac{k_x}{2})}{\sqrt{\cos^2(\frac{k_x}{2}) + \cos^2(\frac{k_y}{2}) + E_+^2}} \end{bmatrix}, \begin{bmatrix} \frac{\cos(\frac{k_y}{2})}{\sqrt{\cos^2(\frac{k_x}{2}) + \cos^2(\frac{k_y}{2}) + E_-^2}} \\ \frac{\cos(\frac{k_x}{2})}{\sqrt{\cos^2(\frac{k_x}{2}) + \cos^2(\frac{k_y}{2}) + E_-^2}} \end{bmatrix} \quad (5.4)$$

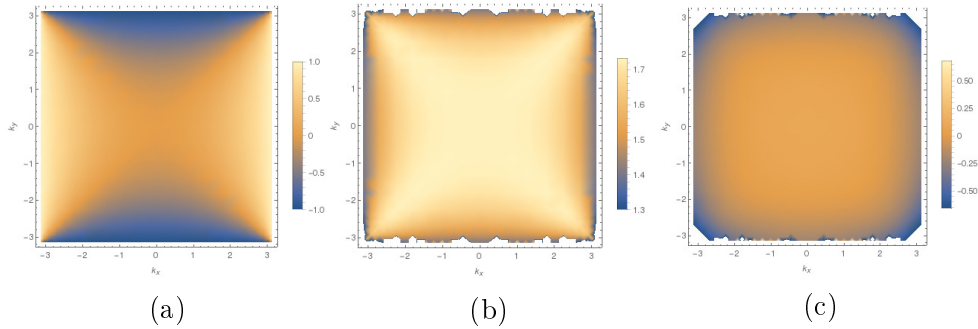


Figure 5.3: Eigenvector for a)the middle band b)lower band c)top band for staggered case case with  $t' = 0.75$  and  $V_1 = V_3 = 0, V_2 = 1$

The eigen-vectors show that that the inversion symmetry is there. One can also get the Wannier states by calculating the Fourier transform of the eigenvectors. This will give us the real space shapes of the orbitals. Now, we will investigate the symmetric case( $t' = 0.75, V_1 = V_2 = V_3 =$

1). In this case, we have Dirac point. The eigen values are  $E_1 = V + 2\sqrt{t^2 \cos^2(\frac{k_x a}{2}) + t^2 \cos^2(\frac{k_y a}{2})}$ ,  $E_2 = V - 2\sqrt{t^2 \cos^2(\frac{k_x a}{2}) + t^2 \cos^2(\frac{k_y a}{2})}$ ,  $E_3 = V$

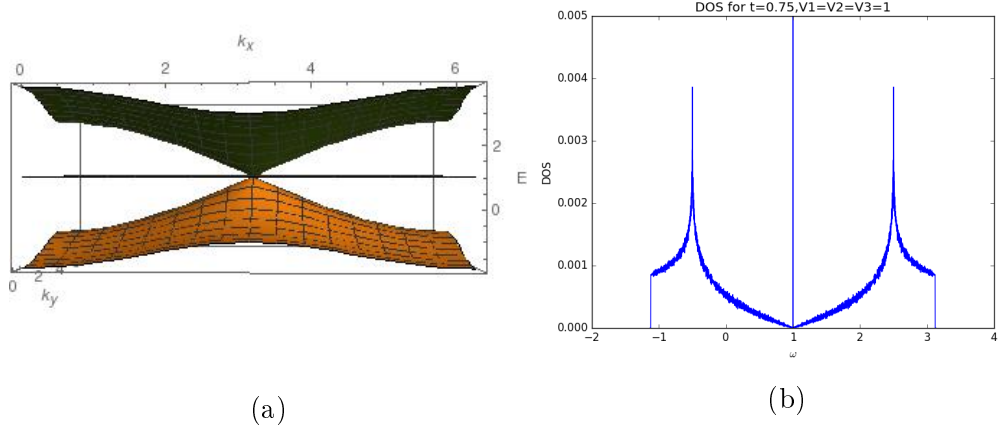


Figure 5.4: a) Band dispersion of the ‘a’ bands in region  $[0, 2\pi]$  and (b) density of states for symmetric case with  $t = 0.75, V_1 = V_2 = V_3 = 1$

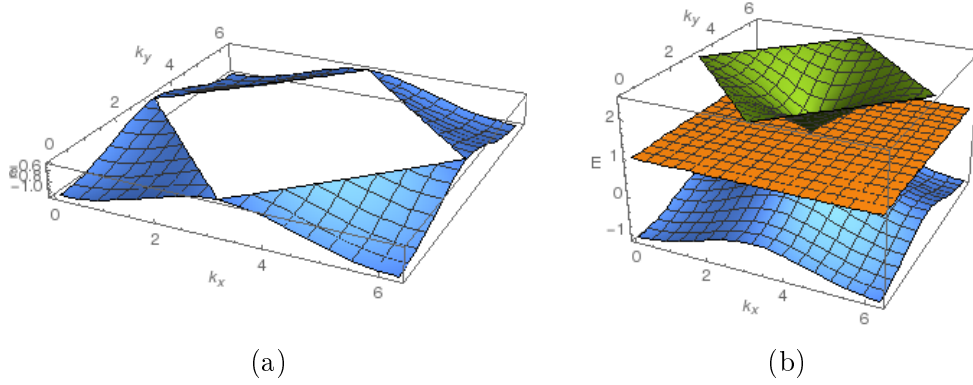


Figure 5.5: Fermi surface for Von-Hove singularity a) at  $\omega = -0.5$  and b)  $\omega = 2.5$  ( $t = 0.75, V_1 = V_2 = V_3 = 1$ )

The corresponding eigenvectors are:

$$\frac{1}{\sqrt{2}} \begin{bmatrix} 1 \\ \frac{\cos(\frac{k_x a}{2})}{\sqrt{\cos^2(\frac{k_x a}{2}) + \cos^2(\frac{k_y a}{2})}} \\ \frac{\cos(\frac{k_y a}{2})}{\sqrt{\cos^2(\frac{k_x a}{2}) + \cos^2(\frac{k_y a}{2})}} \end{bmatrix}, \frac{1}{\sqrt{2}} \begin{bmatrix} -1 \\ \frac{\cos(\frac{k_x a}{2})}{\sqrt{\cos^2(\frac{k_x a}{2}) + \cos^2(\frac{k_y a}{2})}} \\ \frac{\cos(\frac{k_y a}{2})}{\sqrt{\cos^2(\frac{k_x a}{2}) + \cos^2(\frac{k_y a}{2})}} \end{bmatrix}, \begin{bmatrix} 0 \\ \frac{\cos(\frac{k_y a}{2})}{\sqrt{\cos^2(\frac{k_x a}{2}) + \cos^2(\frac{k_y a}{2})}} \\ \frac{\cos(\frac{k_x a}{2})}{\sqrt{\cos^2(\frac{k_x a}{2}) + \cos^2(\frac{k_y a}{2})}} \end{bmatrix} \quad (5.5)$$

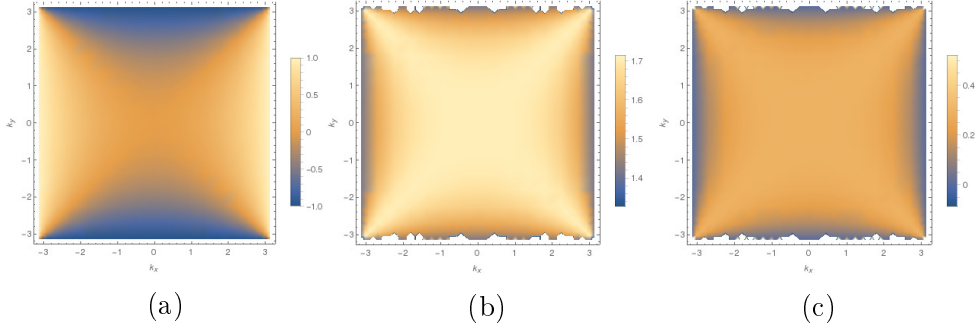


Figure 5.6: Eigenvector for a)the middle band b)lower band c)top band for symmetric case with  $t' = 0.75$  and  $V_1 = V_2 = V_3 = 1$

If we consider a point in the momentum space, say  $(k_x, k_y)$ . If we invert about the  $k_y$  axis,  $k_x \rightarrow -k_x$ ,  $f(k_x) = f(-k_x)$  where  $f$  is the function under consideration. So, the eigenvectors has  $\cos(k)$  in its component and we know  $\cos$  is an even function. So, the eigenvectors will have inversion symmetry. From the figures above, it can be verified that the inversion symmetry is there.

We want to remove the macroscopic degeneracy. So we introduce next nearest neighbour interactions. The stability of the band touching points can be checked by introducing the next nearest hopping. Let  $t'$  be the next nearest hopping parameter. The next nearest hopping is the diagonal hopping between sites 1 and 3. Also at the same time,  $t''$  hopping is introduced, which is the hopping from one edge centre to the center of opposite edge i.e. from site 1 in one unit cell to site 1 in adjacent unit cells and site 3 in one unit cell to site 3 in its adjacent unit cells. in The tight binding Hamiltonian matrix for the non interacting fermions in momentum space is

$$H(k) = \begin{bmatrix} V_1 - t'' \cos(k_x a) & -2t \cos\left(\frac{k_y}{2}\right) & -4t' \cos\left(\frac{k_y a}{2}\right) \cos\left(\frac{k_x a}{2}\right) \\ -2t \cos\left(\frac{k_y}{2}\right) & V_2 & -2t \cos\left(\frac{k_x}{2}\right) \\ -4t' \cos\left(\frac{k_y a}{2}\right) \cos\left(\frac{k_x a}{2}\right) & -2t \cos\left(\frac{k_x}{2}\right) & V_3 - t'' \cos(k_y a) \end{bmatrix} \quad (5.6)$$

We will begin with the symmetric case first i.e. all the on-site potentials are same i.e.  $V_1 = V_2 = V_3 = 1$ .

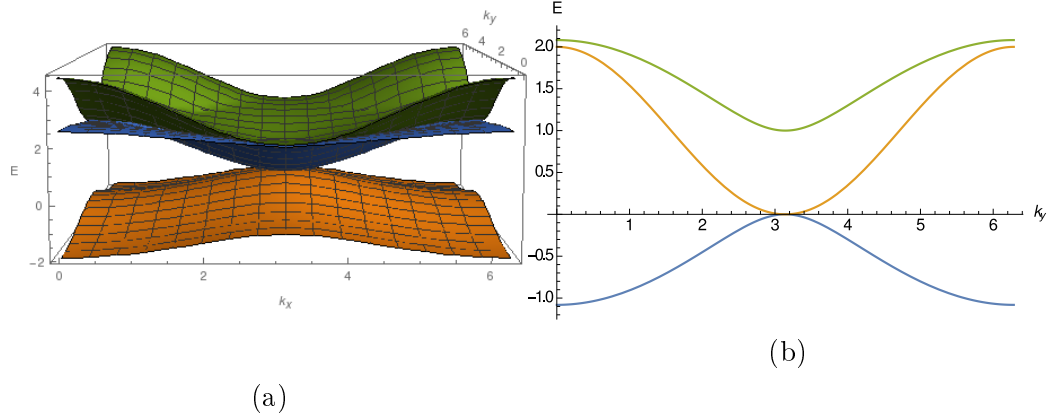


Figure 5.7: a) Band structure for symmetric case for electrons in  $a$  orbital with parameters  $t = 0.75, t' = 0.6, t'' = -0.5$ , (b) Cross section of the band dispersions in fig(a) for  $a$  orbital electrons through plane  $k_x = \pi$

The quadratic band crossing point still remains. It remains unaffected by additional hoppings as expected. The additional hoppings introduced in the system doesn't break any symmetry which protects the QBCP. Now if we look at the cross section of the band structure along the plane  $k_x = k_y$ , two anisotropic Dirac points can be seen. There are four such points because of the four fold symmetry. The anisotropic Dirac points have different Fermi velocity along different directions. There are two Von-Hove singularity in the density of states.

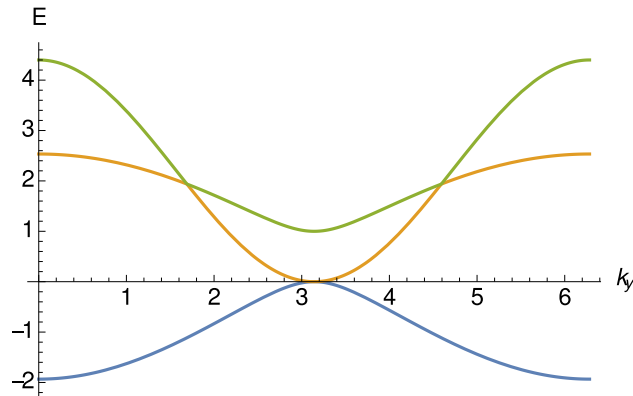


Figure 5.8: Cross section of the band structure for  $a$  orbital through the plane  $k_x = k_y$  with parameters  $t = 0.75, t' = 0.6, t'' = -0.5$

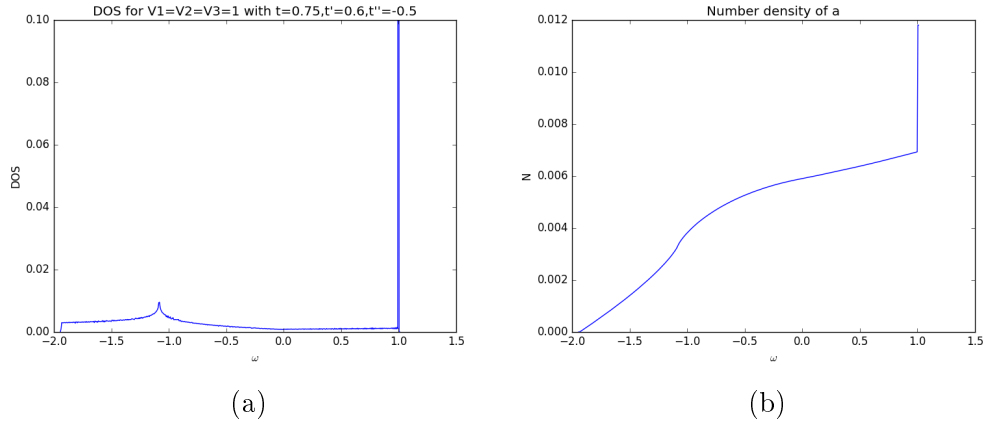


Figure 5.9: a)DOS for symmetric case for  $a$  bands with  $(t = 0.75, t' = 0.6, t'' = -0.5)$ , (b)Number density for symmetric case for  $a$  bands for the DOS in fig(a)

Similarly, the band dispersions, density of states for staggered cases with  $V_1 = V_3 = 0, V_2 = 1$  are also plotted.

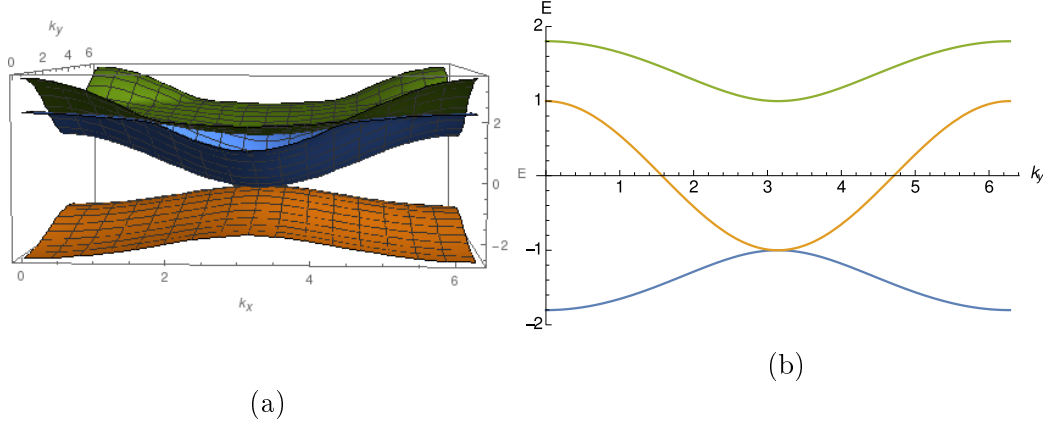


Figure 5.10: a)Band structure for staggered case for electrons in  $a$  orbital with parameters  $V_1 = V_3 = 0, V_2 = 1, t = 0.75, t' = 0.6, t'' = -0.5$ , (b)Cross section of the band dispersions in fig(a) for  $a$  orbital electrons through plane  $k_x = \pi$

There is a quadratic band crossing point(QBCP) at  $(\pi, \pi)$ . It is clear from the figure above that introduction of additional hopping doesn't have any effect of the QBCP. It remains as it was without additional hoppings. However, the flat band becomes dispersive. Both diagonal hopping and the

hopping from one edge center to the opposite edge center doesn't break the four-fold symmetry. So, looking at the cross sectional plane  $k_x = \pi$  will give us information about  $k_y = \pi$  plane since rotation by  $\pi$  doesn't change anything.

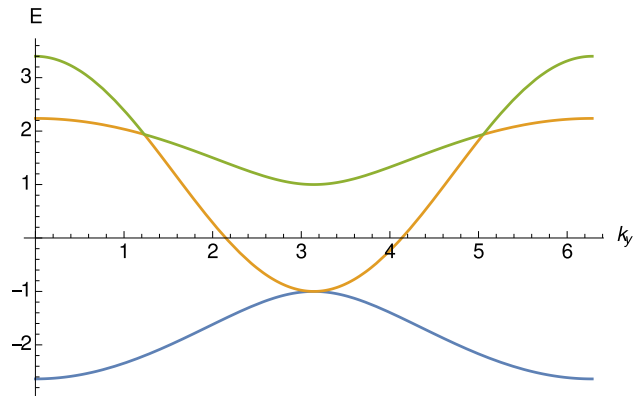


Figure 5.11: Cross section of the band dispersions for  $a$  through the diagonal plane  $k_x = k_y$  with parameters  $V_1 = V_3 = 0, V_2 = 1, t = 0.75, t' = 0.6, t'' = -0.5$

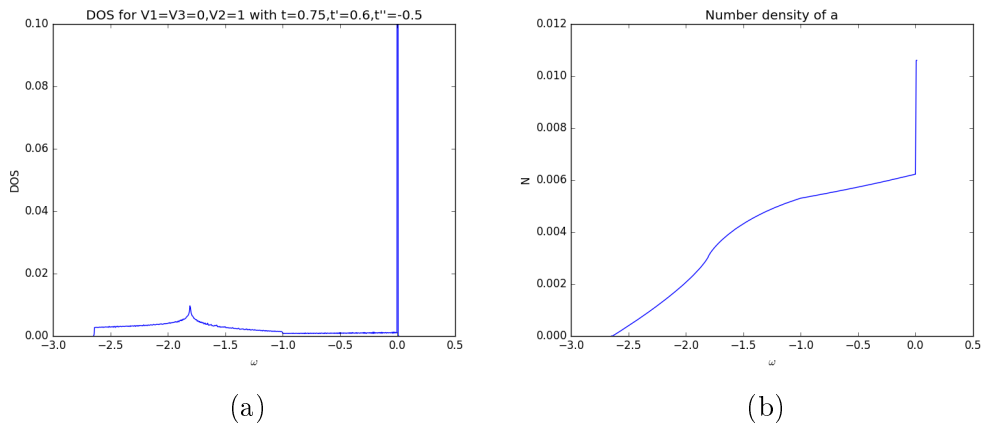


Figure 5.12: a)DOS for staggered case for  $a$  bands with  $(t = 0.75, t' = 0.6, t'' = -0.5)$ , (b)Number density for staggered case for  $a$  bands for the DOS in fig(a)

Now we introduce mixing between the orbitals -  $a$  and  $b$ . However the mixing is non-local i.e. the orbital " $b$ " at position 1 mixes with orbital " $a$ " at positions 2 and vice-versa. Similar is the mixing between site 2 and site

3. This is done in order to map it to the mixing of  $a_+$  and  $a_-$  in the dimer model.

$$\begin{pmatrix} V_1 - 2t'' \cos(k_x a) & -4t \cos\left(\frac{k_y a}{2}\right) & -4t' \cos\left(\frac{k_y a}{2}\right) \cos\left(\frac{k_x a}{2}\right) & 0 & 0 & 0 \\ -4t \cos\left(\frac{k_y a}{2}\right) & V_2 & -4t \cos\left(\frac{k_x a}{2}\right) & i \sin\left(\frac{k_y a}{2}\right) & 0 & i \sin\left(\frac{k_x a}{2}\right) \\ -4t' \cos\left(\frac{k_y a}{2}\right) \cos\left(\frac{k_x a}{2}\right) & -4t \cos\left(\frac{k_x a}{2}\right) & V_3 - 2t'' \cos(k_y a) & 0 & 0 & 0 \\ 0 & -i \sin\left(\frac{k_y a}{2}\right) & 0 & V_1 & 0 & 0 \\ 0 & 0 & 0 & 0 & V_2 & 0 \\ 0 & -i \sin\left(\frac{k_x a}{2}\right) & 0 & 0 & 0 & V_3 \end{pmatrix} \quad (5.7)$$

We plot the eigenvalues to get the band structure. In this case, since there is an orbital mixing, we expect that the b bands won't be dispersionless anymore. They will acquire dispersion.

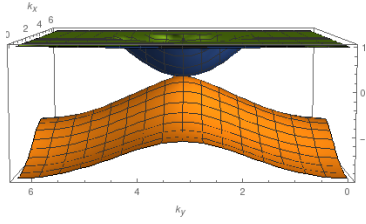


Figure 5.13: Dispersion relation for symmetric case for  $a$  bands with  $(t = 0.75, t' = 0.6, t'' = -0.5)$

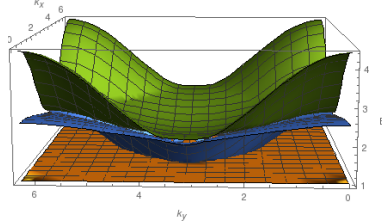


Figure 5.14: Dispersion relation for symmetric case for  $b$  bands with  $(t = 0.75, t' = 0.6, t'' = -0.5)$

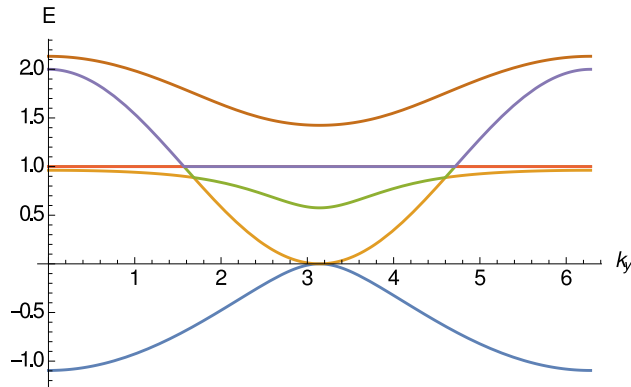


Figure 5.15: Cross section of the band dispersions for all bands through the plane  $k_x = \pi$  with parameters  $t = 0.75, t' = 0.6, t'' = -0.5, V_1 = V_2 = V_3 = 1$

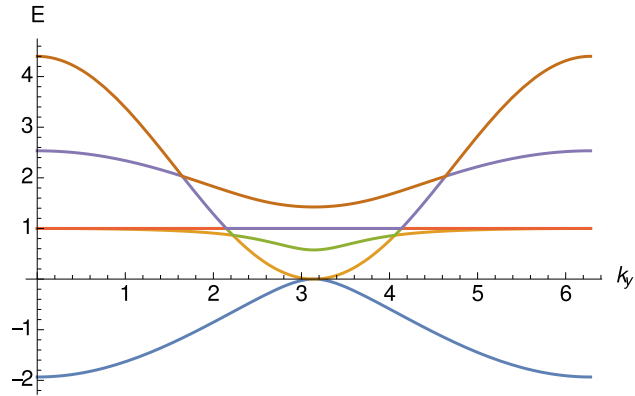


Figure 5.16: Cross section of the band dispersions for all bands through the plane  $k_x = k_y$  with parameters  $t = 0.75, t' = 0.6, t'' = -0.5, V_1 = V_2 = V_3 = 1$

From the band structure, it is clear that the QBCP still remains. Mixing of the orbitals doesn't break any symmetry. Hence, the QBCP is stable even if there is mixing. The QBCP is in the 'a' orbital bands. The cross section along the plane  $k_x = \pi$  shows that there are two anisotropic Dirac cones in each side while along the plane  $k_x = k_y$ , there are three.

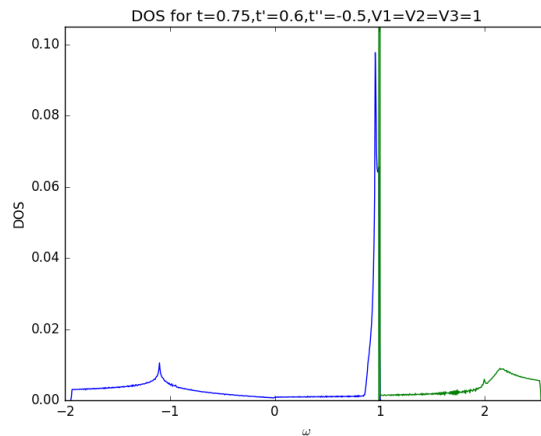


Figure 5.17: DOS for the symmetric case with  $t=0.75, t''=0.6, t'=-0.5$



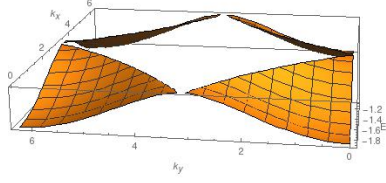


Figure 5.18: Fermi surface for symmetric case for a with ( $t = 0.75, t' = 0.6, t'' = -0.5$ ) for Von-Hove singularity at  $\omega = -1.099$

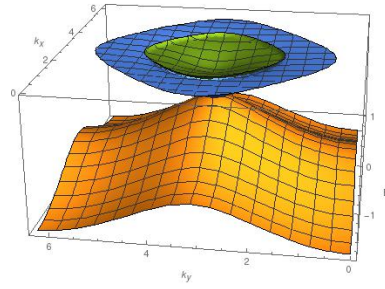


Figure 5.19: Fermi surface for symmetric case for a with ( $t = 0.75, t' = 0.6, t'' = -0.5$ ) for Von-Hove singularity at  $\omega = 0.95683$

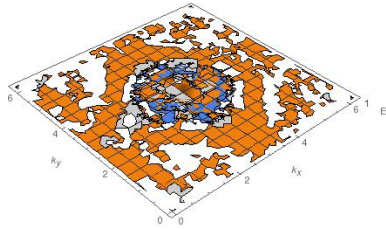


Figure 5.20: Fermi surface for symmetric case for b with ( $t = 0.75, t' = 0.6, t'' = -0.5$ ) for Von-Hove singularity at  $\omega = 0.99684$

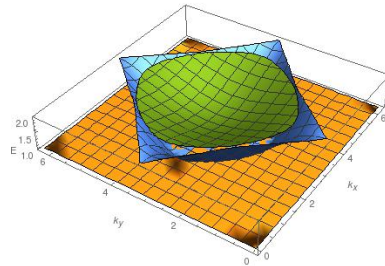


Figure 5.21: Fermi surface for symmetric case for b with ( $t = 0.75, t' = 0.6, t'' = -0.5$ ) for Von-Hove singularity at  $\omega = 2.0023$

We will look at the staggered case with the same parameter set and orbital mixing where the mixing strength is 0.3

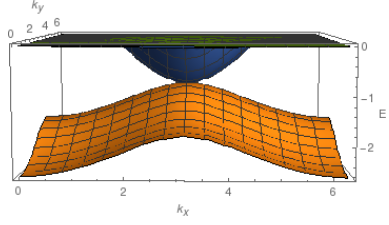


Figure 5.22: Dispersion relation for symmetric case for  $a$  bands with  $(t = 0.75, t' = 0.6, t'' = -0.5)$

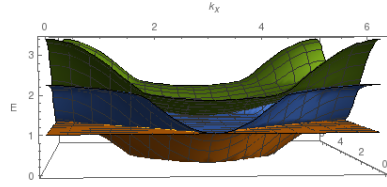


Figure 5.23: Dispersion relation for staggered case for  $b$  bands with  $(t = 0.75, t' = 0.6, t'' = -0.5)$

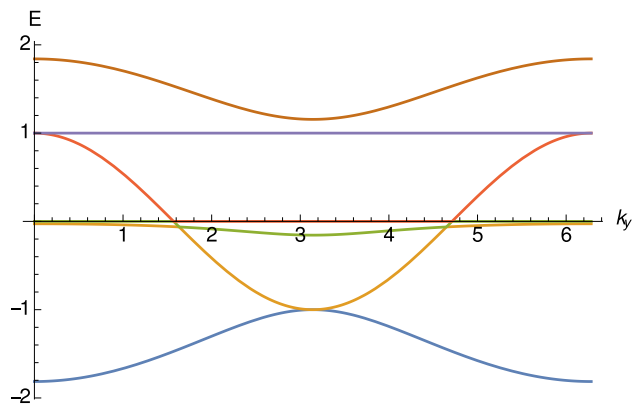


Figure 5.24: Cross section of the band dispersions for all bands through the plane  $k_x = \pi$  with parameters  $t = 0.75, t' = 0.6, t'' = -0.5, V_1 = V_3 = 0, V_2 = 1$

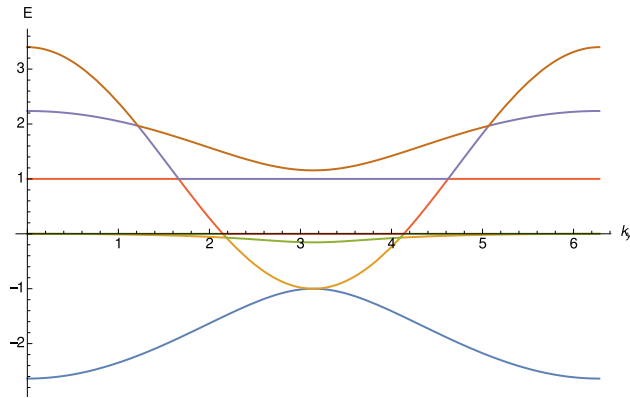


Figure 5.25: Cross section of the band dispersions for all bands through the diagonal plane  $k_x = k_y$  with parameters  $t = 0.75, t' = 0.6, t'' = -0.5, V_1 = V_3 = 0, V_2 = 1$

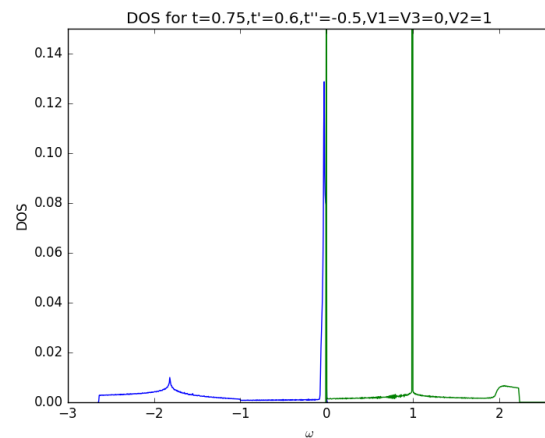


Figure 5.26: DOS for the staggered case with  $t=0.75, t''=0.6, t'''=-0.5, V_1=V_3=0, V_2=1$

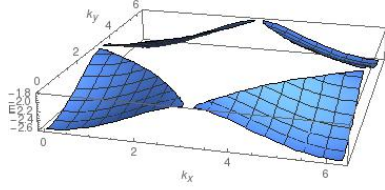


Figure 5.27: Fermi surface for staggered case for lower bands with  $(t = 0.75, t' = 0.6, t'' = -0.5)$  for Von-Hove singularity at  $\omega = -1.8182$

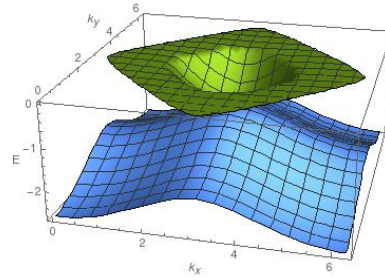


Figure 5.28: Fermi surface for staggered case for lower bands with  $(t = 0.75, t' = 0.6, t'' = -0.5)$  for Von-Hove singularity at  $\omega = -0.0272$

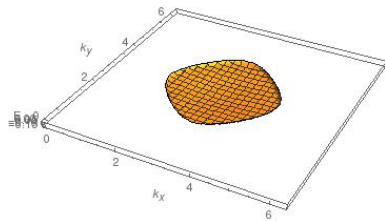


Figure 5.29: Fermi surface for staggered case for top bands with  $(t = 0.75, t' = 0.6, t'' = -0.5)$  for Von-Hove singularity at  $\omega = -0.00316$

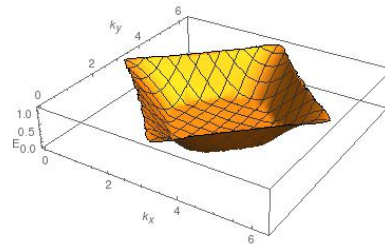


Figure 5.30: Fermi surface for staggered case for top bands with  $(t = 0.75, t' = 0.6, t'' = -0.5)$  for Von-Hove singularity at  $\omega = 0.99548$

Lastly, one can extend this two dimensional Lieb lattice model with dimers to three dimensions. Each layer is stacked over the other. This is done in a fashion such that the vertical hopping is only between the dimers at position 2. The extension would give us an insight into whether the system would be in a strong topological insulator or weak topological insulator. In three dimensions, there are four  $Z_2$  invariants[2] which one has to calculate.

# Chapter 6

## Discussion

In the previous chapter, all the results have been compiled according to the various cases. The model with a dimer on each site of a Lieb lattice supports Dirac cones when the on-site potentials are equal. For the staggered configuration, we get a quadratic band crossing point at  $(\pi, \pi)$  which is the edge of the first Brillouin zone. One important thing to notice is that we haven't considered spin-orbit coupling in the first case. The three bands touching together for the  $a_+$  species is a special case because it is possible only when a) the inter-dimer hopping amplitudes are equal, b) there is four-fold symmetry, and c) no spin orbit coupling [20]. Both the BCPs have non-zero Berry phase. So, these are topologically non-trivial points.

Once diagonal hoppings are introduced in the Hamiltonian, the flat band disperses. However, the point where the three bands touch still survives because none of the conditions mentioned above is broken. This kind of behaviour has been seen in  $K_4$  crystal where isotropic Dirac cones emerge [17]. The band touching point will now be pseudospin-1 Dirac cone since there are three bands which touch and are degenerate at a point.

Due to additional hopping,  $a_-$  starts to hop. When there is only diagonal hopping,  $a_-$  hops by hybridising with  $a_+$ . The  $a_-$  converts into an  $a_+$  and then  $a_+$  hops. The next thing to observe is that many of the Fermi surfaces at Von-Hove singularities have electron and hole pockets. There are cases in which there is Fermi surface nesting. Then there will be nesting instability depending on the filling. If the band is partially filled, then the most dominant instability may be a superconducting instability. There can be various other instabilities. The anisotropic Dirac cones that we have seen in the band structure can also be found in real systems [15].

The next thing to notice would be the effect of electric field. Electric

field induces a hybridisation or mixing between the  $a_+$  and  $a_-$  fermions. It breaks the inversion symmetry. Because of this reason, gaps open at the Dirac points. Rashba effect is present in a system when the inversion symmetry is broken. It may be due to electric field or if the crystal itself lacks the symmetry.

The two orbital model also hosts some of the interesting topological features of the dimer model. The two orbital on each Lieb lattice system may be seen in some materials. One of the orbital may be s, which is even under parity. Then the other may be p or f. It is also possible to have a (p,d) combination.

## 6.1 Mean-field Theory

The effects of interaction can be studied using mean field theory. The Hamiltonian in the momentum can be written as

$$H = \sum_k [\varepsilon_+(k)a_{+k}^\dagger a_{+k} + \varepsilon_-(k)a_{-k}^\dagger a_{-k}] + V \sum_\mu n_{a+\mu} n_{a-\mu} \quad (6.1)$$

where  $n_{a+\mu} = a_{+\mu}^\dagger a_{+\mu}$ . The interaction term is the one which makes it difficult to solve the Hamiltonian. We use Wick's theorem to decouple the interaction term. The Wick's theorem will consider all the possible pairings of creation and annihilation operator.

$$a_+^\dagger a_+ a_-^\dagger a_- = (a_+^\dagger a_+)(a_-^\dagger a_-) - (a_+^\dagger a_-)(a_-^\dagger a_+) \quad (6.2)$$

Now because of the electric field,  $\langle a_+^\dagger a_- \rangle \neq 0$ . We define order parameters  $\Delta_0 = \langle a_+^\dagger a_- \rangle = \Delta e^{i\theta}$ . This is the excitonic order parameter. We also define  $\Delta_1 = \langle a_+^\dagger a_+ \rangle, \Delta_2 = \langle a_-^\dagger a_- \rangle$ .

$$n_{a_+} n_{a_-} = (n_{a_+} - \Delta_1 + \Delta_1)(n_{a_-} - \Delta_2 + \Delta_2) \quad (6.3)$$

$$= -\Delta_1 \Delta_2 + a_+^\dagger a_+ \Delta_2 + a_-^\dagger a_- \Delta_1 \quad (6.4)$$

Here we have neglected the fluctuations. If we define a spinor  $\Psi^\dagger = (a_+^\dagger, a_-^\dagger)$ , the first term in the Wick decoupling can be written as

$$I_1 = -\Delta_1 \Delta_2 + \begin{bmatrix} a_+^\dagger & a_-^\dagger \end{bmatrix} \begin{bmatrix} \Delta_2 & 0 \\ 0 & \Delta_1 \end{bmatrix} \begin{bmatrix} a_+ \\ a_- \end{bmatrix} \quad (6.5)$$

We can define  $m_z = \Delta_1 - \Delta_2$  and  $m_0 = \Delta_1 + \Delta_2$ .

$$m_z = \langle a_+^\dagger a_+ - a_-^\dagger a_- \rangle = [a_+^\dagger \quad a_-^\dagger] \begin{bmatrix} 1 & 0 \\ 0 & -1 \end{bmatrix} \begin{bmatrix} a_+ \\ a_- \end{bmatrix} = \langle \Psi^\dagger \sigma_z \Psi \rangle \quad (6.6)$$

$$m_0 = \langle a_+^\dagger a_+ + a_-^\dagger a_- \rangle = [a_+^\dagger \quad a_-^\dagger] \begin{bmatrix} 1 & 0 \\ 0 & 1 \end{bmatrix} \begin{bmatrix} a_+ \\ a_- \end{bmatrix} = \langle \Psi^\dagger \sigma_0 \Psi \rangle \quad (6.7)$$

where  $\sigma_0$  is the identity matrix. Re-writing  $I_1$  in terms of  $m_z, m_0, \Psi$  and Pauli matrices we get

$$I_1 = \frac{m_z^2 - m_0^2}{4} + \frac{m_0 \Psi^\dagger \sigma_0 \Psi}{2} - \frac{m_z \Psi^\dagger \sigma_z \Psi}{2} \quad (6.8)$$

$$= \left( \frac{m_z^2}{4} - \frac{m_z \Psi^\dagger \sigma_z \Psi}{2} \right) - \left( \frac{m_0^2}{4} - \frac{m_0 \Psi^\dagger \sigma_0 \Psi}{2} \right) \quad (6.9)$$

For the second term in the Wick decoupling, we get

$$I_2 = (a_+^\dagger a_-)(a_-^\dagger a_+) \quad (6.10)$$

$$= (a_+^\dagger a_- - \Delta_0 + \Delta_0)(a_-^\dagger a_+ - \Delta_0^* + \Delta_0^*) \quad (6.11)$$

$$= -|\Delta_0|^2 + a_+^\dagger a_- \Delta_0^* + a_-^\dagger a_+ \Delta_0 \quad (6.12)$$

$$= -|\Delta_0|^2 + \Psi^\dagger \begin{bmatrix} 0 & \Delta_0^* \\ \Delta_0 & 0 \end{bmatrix} \Psi \quad (6.13)$$

Similar to  $m_0, m_z$ , we define

$$m_x = \Delta_0 + \Delta_0^* = \langle a_+^\dagger a_- + a_-^\dagger + a_+ \rangle = \langle \Psi^\dagger \sigma_x \Psi \rangle \quad (6.14)$$

$$m_y = -i(\Delta_0 - \Delta_0^*) = -i \langle a_+^\dagger a_- - a_-^\dagger + a_+ \rangle = \langle \Psi^\dagger \sigma_y \Psi \rangle \quad (6.15)$$

If we go to the original  $c_a, c_b$  dimer basis,  $m_x = \langle n_a - n_b \rangle_\mu$ . This is the polarization on each bond  $\mu$ . On the other hand,  $m_y = i \langle c_a^\dagger c_b - c_b^\dagger c_a \rangle_\mu$ . Using  $m_x$  and  $m_y$ ,  $I_2$  can be written as

$$I_2 = -\frac{m_x^2 + m_y^2}{4} + \Psi^\dagger \left( \frac{m_x}{2} \sigma_x + \frac{m_y}{2} \sigma_y \right) \Psi \quad (6.16)$$

Using this form of  $I_1$  and  $I_2$ , the mean field Hamiltonian can be written as

$$H = \sum_k \Psi_k^\dagger H_0(k) \Psi_k - \frac{U}{2} \sum_\mu \Psi_\mu^\dagger (m_x \sigma_x + m_y \sigma_y + m_z \sigma_z) \Psi_\mu + \frac{U}{4} (m_x^2 + m_y^2 + m_z^2) \quad (6.17)$$

The next step would be to get the mean field free energy. The gap equations can be obtained by minimizing  $F$  with respect to the order parameters  $\Delta_i$  i.e.  $\frac{\partial F}{\partial \Delta_i} = 0$ . This is what is going to be done next.

# References

- [1] communication with mukul laad and luis craco.
- [2] Liang Fu and C. L. Kane. Topological insulators with inversion symmetry. *Phys. Rev. B*, 76:045302, Jul 2007.
- [3] Maxim Dzero, Kai Sun, Victor Galitski, and Piers Coleman. Topological kondo insulators. *Phys. Rev. Lett.*, 104:106408, Mar 2010.
- [4] Gerald D Mahan. Many particle physics.
- [5] M. V. Berry. Quantal phase factors accompanying adiabatic changes. *Proceedings of the Royal Society of London A: Mathematical, Physical and Engineering Sciences*, 392(1802):45–57, 1984.
- [6] E. Müller-Hartmann. The hubbard model at high dimensions: some exact results and weak coupling theory. *Zeitschrift für Physik B Condensed Matter*, 76(2):211–217, 1989.
- [7] E. Müller-Hartmann. Correlated fermions on a lattice in high dimensions. *Zeitschrift für Physik B Condensed Matter*, 74(4):507–512, 1989.
- [8] D N Zubarev. Double-time green functions in statistical physics. *Soviet Physics Uspekhi*, 3(3):320, 1960.
- [9] C Lacroix. Density of states for the anderson model. *Journal of Physics F: Metal Physics*, 11(11):2389, 1981.
- [10] M. O. Goerbig, J.-N. Fuchs, G. Montambaux, and F. PiÅchon. Electric-field-induced lifting of the valley degeneracy in  $\text{Îs}-(\text{bedt-ttf})_2$  i 3 dirac-like landau levels. *EPL (Europhysics Letters)*, 85(5):57005, 2009.
- [11] U. Brandt and C. Mielsch. Thermodynamics and correlation functions of the falicov-kimball model in large dimensions. *Zeitschrift für Physik B Condensed Matter*, 75(3):365–370, 1989.



- [12] U. Brandt and C. Mielsch. Free energy of the falicov-kimball model in large dimensions. *Zeitschrift für Physik B Condensed Matter*, 82(1):37–41, 1991.
- [13] Antoine Georges and Gabriel Kotliar. Hubbard model in infinite dimensions. *Phys. Rev. B*, 45:6479–6483, Mar 1992.
- [14] Kai Sun, Hong Yao, Eduardo Fradkin, and Steven A. Kivelson. Topological insulators and nematic phases from spontaneous symmetry breaking in 2d fermi systems with a quadratic band crossing. *Phys. Rev. Lett.*, 103:046811, Jul 2009.
- [15] Joonbum Park, G. Lee, F. Wolff-Fabris, Y. Y. Koh, M. J. Eom, Y. K. Kim, M. A. Farhan, Y. J. Jo, C. Kim, J. H. Shim, and J. S. Kim. Anisotropic dirac fermions in a bi square net of srmnbi<sub>2</sub>. *Phys. Rev. Lett.*, 107:126402, Sep 2011.
- [16] Laad et. al. First-principles correlated approach to the normal state of strontium ruthenate.
- [17] Masahisa Tsuchiizu. Three-dimensional higher-spin dirac and weyl dispersions in the strongly isotropic  $K_4$  crystal. *Phys. Rev. B*, 94:195426, Nov 2016.
- [18] Martin Wilkens. Quantum phase of a moving dipole. *Phys. Rev. Lett.*, 72:5–8, Jan 1994.
- [19] F. D. M. Haldane. Model for a quantum hall effect without landau levels: Condensed-matter realization of the "parity anomaly". *Phys. Rev. Lett.*, 61:2015–2018, Oct 1988.
- [20] Wei-Feng Tsai, Chen Fang, Hong Yao, and Jiangping Hu. Interaction-driven topological and nematic phases on the lieb lattice. *New Journal of Physics*, 17(5):055016, 2015.